# MIT Open Access Articles

## *JINAbase—A Database for Chemical Abundances of Metal-poor Stars*

**Massachusetts Institute of Technology**

CrossMark

# JINAbase—A Database for Chemical Abundances of Metal-poor Stars

Abdu Abohalima[1,2] and Anna Frebel[1,2]
[1] Department of Physics and Kavli Institute for Astrophysics and Space Research, Massachusetts Institute of Technology, Cambridge, MA, USA; afrebel@mit.edu
[2] Joint Institute for Nuclear Astrophysics (JINA)—Center for the Evolution of the Elements, East Lansing, MI, USA

## Abstract

Reconstructing the chemical evolution of the Milky Way is crucial for understanding the formation of stars, planets, and galaxies throughout cosmic time. Different studies associated with element production in the early universe and how elements are incorporated into gas and stars are necessary to piece together how the elements evolved. These include establishing chemical abundance trends, as set by metal-poor stars, comparing nucleosynthesis yield predictions with stellar abundance data, and theoretical modeling of chemical evolution. To aid these studies, we have collected chemical abundance measurements and other information, such as stellar parameters, coordinates, magnitudes, and radial velocities, for extremely metal-poor stars from the literature. The database, JINAbase, contains 1659 unique stars, 60% of which have $[\mathrm{Fe/H}] \leqslant -2.5$. This information is stored in an SQL database, together with a user-friendly queryable web application (http://jinabase.pythonanywhere.com). Objects with unique chemical element signatures (e.g., *r*-process stars, *s*-process and CEMP stars) are labeled or can be classified as such. We find that the various neutron-capture element signatures occur in up to 19% of metal-poor stars with $[\mathrm{Fe/H}] \leqslant -2.0$, and 32% when also considering carbon enhancement. The web application enables fast selection of customized comparison samples from the literature for the aforementioned studies and many more. Using multiple entries for three of the most well-studied metal-poor stars, we evaluate systematic uncertainties of chemical abundance measurements between the different studies. We provide a brief guide to the selection of chemical elements for model comparisons for non-spectroscopists who wish to learn about metal-poor stars and the details of chemical abundance measurements.

*Key words:* astronomical databases: miscellaneous – catalogs – nuclear reactions, nucleosynthesis, abundances – stars: abundances – stars: Population II

## 1. Introduction

Metal-poor stars, broadly defined, are stars with a heavy element content less than 1/10th that of the Sun (Beers & Christlieb 2005). They are generally classified as old Population II (Pop II) stars and predominantly reside in the halo of the Milky Way (e.g., Beers et al. 2000; Carollo et al. 2007), although a few stars have by now also been discovered in the bulge (e.g., Howes et al. 2015). Satellite dwarf spheroidal galaxies also contain metal-poor stars (e.g., Cohen et al. 2008), and in particular, the ultra-faint dwarfs contain exclusively metal-poor stars (e.g., Frebel et al. 2014) given their short star formation and enrichment history. The most metal-poor stars are thought to have formed from gas only enriched by the very first stars, also called Population III stars (Pop III). These metal-free, massive, short-lived stars are believed to have formed a few hundred million years after the Big Bang (e.g., Bromm & Larson 2004; O'Shea & Norman 2007) and were responsible for the first metal enrichments of the interstellar medium (ISM). This gave rise to the formation of the first Pop II stars (e.g., Greif et al. 2010; Wise et al. 2012; Crosby et al. 2013), which contain the chemical signatures of these first supernovae.

Thus, extremely metal-poor stars, defined here as stars with $[\mathrm{Fe/H}] \leqslant -3.0$, have been the focus of many studies as they are an important tool for reconstructing the early chemical history of the universe. Particularly in the last decade, several large-scale Galactic surveys, such as SDSS, SkyMapper, and LAMOST, have been carried out, leading to a rapidly increasing number of known extremely metal-poor stars.

Given that stars preserve the chemical composition of their birth gas cloud in their atmosphere, extremely metal-poor stars provide a unique record of the physical and chemical state of the early universe. In addition, kinematic analysis of their Galactic orbits yields clues to their origin, e.g., from accreted dwarf galaxies. Thus, by studying the chemical abundances of stars with different metallicities, Galactic chemical evolution can be mapped and understood (Matteucci 2012; Nomoto et al. 2013; Minchev et al. 2014; Côté et al. 2017).

Characteristic element signatures found in extremely metal-poor stars can also enable the reconstruction of individual nucleosynthesis processes and events that occurred in the early universe (Frebel et al. 2005; Lugaro et al. 2008; Heger & Woosley 2010; Ishigaki et al. 2014b; Roederer et al. 2016a). Knowledge of those provides critical aid for constraining chemical evolution models, which is a highly complex subject. This also presents the intersection of observations and theory: observers provide metal-poor stars and their abundances and abundance patterns, and theorists use the nucleosynthesis predictions and chemical evolution models to reproduce the data to gain insight into how the Milky Way evolved. It is thus critical that observational results are made readily available for interpretation. In addition, small but important details pertaining to sample selection that are very familiar to observers, such as those about data taking; analysis procedures; which lines, species, and elements to use; relative versus absolute abundances; etc., are often not known to theorists. This can lead to difficulties in using data as intended, and in the worst case, to misinterpretation of the data.

While these challenges need to be individually addressed for each study at hand, we aim in this paper to describe some

common "pitfalls" that theorists might want to consider when using abundance data of metal-poor stars. This stems from an ongoing discussion in the Joint Institute for Nuclear Astrophysics (JINA) community and a desire for closer communication between observers and theorists. To aid in this process, we here present a web-based queryable database called JINAbase that enables interested users to readily use abundance data from metal-poor stars in the literature. Alongside this, we provide commentary on the many different element abundances and specific abundance signatures found in metal-poor stars to guide usage of the output of JINAbase.

JINAbase contains entries of 994 unique metal-poor stars with [Fe/H] ⩽ −2.5 from the bulge, the halo, classical spheroidal dwarf and ultra-faint dwarf galaxies. In addition, 665 stars from the disk and halo with −2.5 < [Fe/H] ⩽ 0 are included. This reflects data collected from the literature up to 2016 July. The abundance and stellar parameter data collected are based on high-resolution (resolving power of $R = \lambda/\Delta\lambda \gtrsim 15{,}000$, with the majority having $R = 30{,}000$–$40{,}000$) spectroscopic studies found in the literature. New results from forthcoming papers can be added by the authors after registering with the web application (web app). Unfortunately, JINAbase cannot offer a homogenized data set, but is simply a collection of literature results. Nevertheless, repeat analyses of many stars will allow, to some extent, a quantification of differences between various studies, and the field as a whole. Overall, it follows in spirit what was presented in Frebel (2010) and is similar to the SAGA database (Suda et al. 2008). However, JINAbase offers a somewhat different functionality that includes labels, classifications, and selection options to put together custom samples as described below.

The paper is organized as follows. In Section 2, we describe the literature data collected, what can be downloaded from JINAbase for individual stars and samples, and we describe the web application's interface in detail and how to query it. We also comment on the subclasses of metal-poor stars using element signature labels. In Section 3, we make use of the body of literature data to present a brief analysis of the systematic differences between studies of metal-poor stars. We do this for three well-studied metal-poor stars in an illustrative way that also quantifies observational uncertainties that could be nominally adopted in comparisons with theoretical models. To assist non-spectroscopists with selecting meaningful customized stellar abundance samples for comparison with model results, in Section 4 we provide comments on various elemental abundances, e.g., regarding measurement challenges, availability in all stars, or local thermodynamic equilibrium (LTE)/non-local thermodynamic equilibrium (NLTE) effects. We summarize in Section 5.

## 2. Retrieving Chemical Abundances from JINAbase

JINAbase was constructed to provide easy and (near) complete access to metal-poor star abundances for the JINA and larger astronomy communities for a variety of projects that require stellar abundances of metal-poor stars for comparison with model predictions or other observational data. We have designed a queryable web app[3] using Python. The web app includes a user-friendly interface enabling easy plotting of various abundances for a sample of stars, with many useful selection criteria, which types of stars to be included or excluded in the sample, and other features.

---

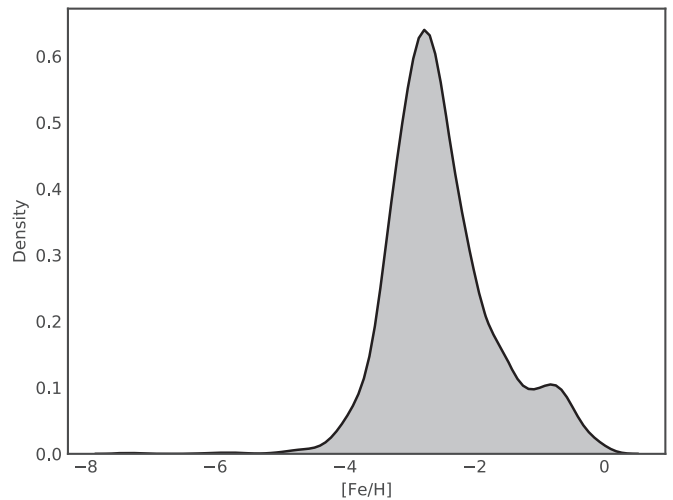3 The web app can be accessed at jinabase.pythonanywhere.com.



**Figure 1.** Metallicity distribution of the stars in JINAbase in the form of a kernel density estimation to visualize the metallicity range covered by the database content. When multiple entries for a given star are available, we chose the one with the largest number of measured elemental abundances; see text for discussion. The main peak in the distribution is at [Fe/H] = −2.75. Any shape for [Fe/H] > −2.5 is likely not physically representative, as the database is increasingly incomplete there. There are two minuscule bumps in the distribution at [Fe/H] ∼ −5.5 and [Fe/H] = −7.3, with the latter actually being nominally included to reflect a star with [Fe/H] < −7.3.

In this section, we describe which data and from where it was collected. We also describe the interface of the web app and the general functionality of JINAbase, how to use it to plot and extract stellar abundances, and how to query it.

### 2.1. Literature Samples Included in JINAbase

We collected chemical abundances and stellar parameters for metal-poor stars (primarily with [Fe/H] ⩽ −2.5) from the period between 1991 and 2016. All references with links to the original papers and their bibtex entries are provided in the web app for easy access. These stars are located in the bulge, the halo, and classical spheroidal dwarf and ultra-faint dwarf galaxies, and are classified as such (although some higher metallicity thick disk stars are included in the halo sample and not separately labeled). Based on studies published before 2016 July JINAbase contains data on 1659 unique stars with [Fe/H] < 0 (with the lowest value being [Fe/H] < −7.3). Given there exist multiple analyses of many stars, a total of 2735 entries are available. HD122563, with 28 entries, is the best studied metal-poor star; see Section 3 for more information. JINAbase contains 857 unique red giants (∼52%), 469 subgiants (∼28%), 54 horizontal branch stars (∼3%), and 279 near-main-sequence turnoff (TO) stars (∼17%). Selection criteria are further described in Section 2.3. These percentages show that observations of metal-poor stars are biased toward red giants, mainly due to the fact that they are observable out to larger distances compared to near main-sequence TO stars.

Figure 1 shows the density kernel smoothed metallicity distribution of the entire sample. For guidance at higher metallicity, i.e., for [Fe/H] > −2, we also added several samples of more metal-rich stars from the thick disk, such as the sample of Fulbright (2000). In JINAbase, they are part of the group halo stars and currently not separately labeled. However, their higher [Fe/H] abundances make them easily identifiable.

The steep decline toward lower metallicities naturally results from these stars being rare. The almost complete cutoff below [Fe/H] = −4.0 illustrates the rarity of the most metal-poor

stars. Only 25 unique stars have [Fe/H] ⩽ −4.0, 8 of which have [Fe/H] ⩽ −4.5, compared to a total of 994 unique stars with [Fe/H] ⩽ −2.5. The sharp dropoff toward higher metallicities is due to selection effects in this literature compilation, as we focused on collecting data for stars with [Fe/H] ⩽ −2.0. Consequently, above [Fe/H] = −2.0, studies are lacking, and in addition, not all stars discovered may have (published) high-resolution abundances. The JINAbase upload feature enables additional stellar abundances and future results, including from higher metallicity stars or globular clusters, to be incorporated.

We also added information on each star taken from the SIMBAD database[4] and Vizier catalogs.[5] This way, coordinates, magnitudes, and radial velocities can be readily extracted from JINAbase together with the stellar parameter and element abundance data. While these are interesting and important quantities that round out the information content of JINAbase, we note that no quality checks or source inspection was done. This should be kept in mind when using the auxiliary information. For example, the radial velocity values listed in SIMBAD may not be the most accurate or latest ones available.

Many different designations usually exist for a given object; in JINAbase we try to give each star a unique identifier to keep track of all entries per star. We identify each star in the SIMBAD database, and then use the main SIMBAD designation as the distinct SIMBAD identifier in JINAbase. This step is of great importance as 437 stars have multiple entries (see Section 3). The name used in the reference for the star is saved in JINAbase as well.

## 2.2. What is Not Included in JINAbase and Cautionary Notes

The primary goal of JINAbase is to provide chemical abundance data as obtained from the various studies in the literature. Accordingly, there naturally are limitations to what JINAbase can provide, as there are multiple intermediate measurements and steps individual to every study that lead to these abundances, such as equivalent width measurements and line lists used. None of these are included in the database (with the exception of the stellar parameters; see below) but can be obtained from the original papers. Neither are measurement uncertainties included here. The reasons are numerous and include the fact that there is currently no homogeneous prescription for determining uncertainties; some studies adopt standard deviations as final uncertainties, others standard errors. Others include and/or assess systematic uncertainties.

For studies wishing to employ abundance uncertainties on the data provided in JINAbase, we recommend consulting with the original papers or to adopt typical uncertainties for high-resolution abundance analysis, as derived in Section 3 from repeat measurements of three metal-poor stars. Alternatively, for a proper and homogeneous assessment of abundance uncertainties, a homogeneous reanalysis of all or at least a large number of stars would need to be undertaken, along the lines of what was done in Yong et al. (2013). Of course, this also pertains to the actual chemical abundances that have been determined in somewhat individual ways by each study. Original papers should always be consulted for further details.

Furthermore, when collecting abundances, we obtain the final or best set of abundances presented. We thus do not

distinguish between LTE and NLTE abundances. But we note that the vast majority of studies report LTE abundances and only some of the more recent ones have begun to provide NLTE stellar parameters and/or abundances. For uploads to the database by registered users, we have implemented a flag on whether LTE or NLTE abundances are being included in the future. All of these inhomogeneities also affect the stellar parameters on which the abundance measurements are based. They have been determined by a variety of methods (e.g., purely spectroscopic, partially based on photometry; different line lists; different analysis codes; etc.) that have not been recorded here. But it is safe to assume that a range of systematic differences arise from using different stellar parameter determination methods.

Finally, the completeness of this literature compilation is nearly impossible to assess, given all of the different samples. Overall, the best guess would be that the completeness level increases with decreasing [Fe/H], given the importance of these stars and regardless of their location (i.e., halo, dwarf galaxy). Assuming that all stars known below [Fe/H] ⩽ −3.5 have published high-resolution abundances available (which, again, may or may not be true), we speculate that JINAbase is complete for these stars. For halo stars with higher [Fe/H], given all the recent survey results, it is clear that this sample is (increasingly) incomplete. This must be taken into account when attempting to reproduce the metallicity distribution function. For dwarf spheroidal galaxies, the situation is similar to that of the halo, with the sample being likely fairly complete up to the [Fe/H] ⩽ −2.0 level and down to a certain magnitude. For ultra-faint dwarf galaxy stars, the situation is likely better. Samples are naturally magnitude limited given the constraints of current telescopes, so that these samples should be fairly complete. In any case, original studies should be consulted to learn more about completeness levels of individual samples.

All in all, the fact is that the entire body of chemical abundances of metal-poor stars is not as homogeneous as one would desire for comparison with, e.g., chemical evolution models. Nevertheless, selecting specific samples, working with abundance ratios, understanding selection effects, and awareness of the associated systematic uncertainties can somewhat alleviate this issue. The goal of this paper is to provide this sort of guidance.

## 2.3. JINAbase Content

An overview of the complete content of JINAbase can be found in Table 1. All or parts of the database can be downloaded, according to chosen selection criteria. In the following, we describe all available information in more detail.

*Labels assigned by JINAbase.* JINAbase assigns an internal ID number for tracking stars. This ID is needed, for example, when plotting abundances versus atomic number.

Following Frebel (2010), JINAbase assigns a priority label to offer the option of plotting a sample in which each point represents one unique star. This is relevant for stars studied by multiple authors, e.g., HD122563. The priority label "1" is given to the study with the most measured abundances. Stars with just one entry are also assigned priority "1." A rough assumption is that a study with more elements reported likely had good or better data than other studies. In the individual case, this may of course not be true, but here, it assists users in making a simple choice to avoid duplicate plotting. Nevertheless, the user has full control over switching this feature on or off.

---

4   http://simbad.u-strasbg.fr/simbad/
5   http://vizier.u-strasbg.fr/viz-bin/VizieR

**Table 1**
JINAbase Content Description

| Data Category | Description |
|---|---|
| Labels assigned by JINAbase | JINAbase ID number |
| | Priority label: to choose from stars with multiple entries |
| | Evolutionary status of star: RG, HB, SG, or MS |
| | Label for carbon enhancement: CR (CEMP), NO (CEMP-no) |
| Literature | Reference code that associates original paper |
| Identifiers | Star name from the respective paper |
| | SIMBAD identifier |
| Labels assigned by authors | NLTE label, label for neutron-capture element enhancement: $r$-I, $r$-II, $r$-lim, $r + s$, $s$- or $i$-rich stars, |
| | Location: halo (HA), bulge (BU), ultra-faint dwarf galaxy (UF), or classical dwarf galaxy (DW) |
| Position | R.A. (J2000) (from SIMBAD) |
| | Decl. (J2000) (from SIMBAD) |
| Radial velocity | Radial velocity (from SIMBAD) |
| | Reference for radial velocity (from SIMBAD) |
| Magnitudes | Values for $U$, $B$, $V$, $R$, $I$, $J$, $H$, $K$ (from SIMBAD) |
| Stellar parameters | Effective temperature, surface gravity, metallicity, microturbulence (from the respective paper) |
| Chemical abundances | $\log \epsilon$ (X), abundances for elements from Li to U, when available |
| | $\log \epsilon$ (X) values for elements with two ionization states (Ca, Ti, Cr, Mn, Fe), when available |

Based on stellar parameters collected from the literature and a 12 Gyr isochrone (Kim et al. 2002), JINAbase assigns a label for the evolutionary status of each star. The following groups are distinguished:

*Red giants:*
   For $[\mathrm{Fe/H}] \geqslant -2.0$: $T_{\mathrm{eff}} \leqslant 5400$ K and $\log g \leqslant 3.5$,
   For $[\mathrm{Fe/H}] \leqslant -2.0$: $T_{\mathrm{eff}} \leqslant 5600$ K and $\log g \leqslant 3.5$,
*Subgiants:*
   For $[\mathrm{Fe/H}] \geqslant -2.0$: $6700 \geqslant T_{\mathrm{eff}} \geqslant 5400$ K, $4.0 \geqslant \log g \geqslant 3.5$,
   For $[\mathrm{Fe/H}] \leqslant -2.0$: $6700 \geqslant T_{\mathrm{eff}} \geqslant 5600$ K, $4.0 \geqslant \log g \geqslant 3.5$,
*Horizontal branch stars:* $T_{\mathrm{eff}} \geqslant 5400$ K, $\log g \leqslant 3.5$,
*Main-sequence TO stars:* $\log g > 4.0$, for all $[\mathrm{Fe/H}]$ and $T_{\mathrm{eff}}$.

In addition, JINAbase assigns labels to carbon-enhanced metal-poor (CEMP) stars. CEMP stars (with enhancement in neutron-capture element abundances) and CEMP-no stars (with *no* enhancement in neutron-capture element abundances) are distinguished, when carbon and barium abundances are available. The physical meaning of these labels is yet to be clarified. For the time being, they serve to classify metal-poor stars. We adopted the definition from Aoki et al. (2007a) for carbon-enhanced stars:

*CEMP:* $[\mathrm{C/Fe}] > 0.7$,

*Literature.* JINAbase assigns a reference code that consists of the first three letters of the name of the first author together with the year of publication, e.g., FRE10.

*Identifiers.* There are two designations for a given star. The one provided by authors of the abundance study and the one

that is the primary SIMBAD identifier (although in some cases, they will be the same). JINAbase records both.

*Labels to be assigned by authors.* When uploading new abundance results, for each star authors are asked to assign a flag indicating whether the abundances are obtained in LTE or NLTE, as well as certain science labels if a given star shows a characteristic abundance signature. For a classification such as an $r$-I, $r$-II, limited $r$-process, $s$-process, $r + s$ rich, or $i$-process star, the abundance pattern of neutron-capture elements should follow the respective pattern, for unambiguous identification. We request adding this label following the abundance ratio criteria given below where we adopt the definition from Beers & Christlieb (2005) and Frebel (2018) for neutron-capture element-enhanced stars:

$r$-I: $0.3 \leqslant [\mathrm{Eu/Fe}] \leqslant +1.0$ and $[\mathrm{Ba/Eu}] < 0.0$,
$r$-II: $[\mathrm{Eu/Fe}] > +1.0$ and $[\mathrm{Ba/Eu}] < 0.0$,
$r$-lim: $[\mathrm{Eu/Fe}] < +0.3$, $[\mathrm{Sr/Ba}] > +0.5$, and $[\mathrm{Sr/Eu}] > 0.0$,
$s$: $[\mathrm{Ba/Fe}] > +1.0$, $[\mathrm{Ba/Eu}] > +0.5$, and $[\mathrm{Ba/Pb}] > -1.5$,
$r + s$: $0.0 < [\mathrm{Ba/Eu}] < +0.5$ and $-1.0 < [\mathrm{Ba/Pb}] < -0.5$,
$i$: $0.0 < [\mathrm{La/Eu}] < 0.6$ and $[\mathrm{Hf/Ir}] \sim +1.0$ (formally "$r/s$" stars; see Beers & Christlieb 2005).
not enhanced, i.e., "normal": $[\mathrm{Ba/Fe}] < 0$.

The $r$-I, $r$-II, and $s$-process star classifications have commonly been used in the literature already. We are adding new classifications to select stars to probe various nucleosynthesis processes beyond the $s$- and $r$-process.

The new "$r$-lim" classification refers to the limited $r$-process (formerly known as the weak $r$-process or LEPP), which is characterized by much decreased second (and third) $r$-process peak element abundances compared to first peak values. The "$r + s$" classification is new following the discovery of the first star that unambiguously shows a combined chemical pattern from the $r$-process and the $s$-process (Gull et al. 2018). Hence, the "$r + s$" label. As more $r + s$ stars are being discovered, this criterion may need to be adjusted; it currently assumes a minimum $r$-process contribution of $[r/\mathrm{Fe}] \sim 0.3$ dex (Frebel 2018). It is slightly different from the "$r/s$" classification of Beers & Christlieb (2005)—the abundance patterns of stars originally called "$r/s$" likely have a different origin, namely from the $i$-process (Hampel et al. 2016). The $i$-process classification is also still being refined as abundance patterns are being modeled with $i$-process yields (F. Herwig 2018, in preparation). We note that more details on these star groups are given in Section 2.4. Additional science labels may also be introduced in the future.

Of note is the following: regarding the classifications of the literature stars using the above criteria, we emphasize here that in order to assign labels systematically to as many stars as possible, we often had to use an abbreviated set of criteria. For the $r$-lim stars we had to leave off the new $[\mathrm{Sr/Eu}]$ criterion, for $s$-process stars we left off the new $[\mathrm{Ba/Pb}]$ criterion, and $i$-process stars were hand-selected following their identification as $i$-process stars in the original papers. The existing abundance data simply did not allow us to meaningfully apply these additional criteria since elements such as Eu or Hf have not been measured in all these stars. Future abundance determinations should aim to measure these additional elements. Only then can the stars be more accurately selected following the criteria presented here. This issue is extensively discussed in Section 2.5 where we apply the abbreviated criteria to

determine meaningful frequencies of stars with the different labels.

Authors are also asked to assign a location label to their stars, such as halo, bulge, ultra-faint dwarf galaxy, or classical dwarf galaxy. This assists in characterizing all Galactic stellar populations as well as the classical and ultra-faint dwarf galaxies that host, e.g., extremely metal-poor stars, and when comparing stellar abundances of different populations.

We distinguish four main locations for metal-poor stars:

*Halo:* the halo of the Galaxy hosts about 90% of all the unique stars included in JINAbase since we deliberately included a few thick disk metal-rich stars for comparison. Among known metal-poor stars with [Fe/H] $\leqslant -3$, 416 out of 439 stars are members of the field halo population of the Galaxy, the remaining 23 stars are located in dwarf galaxies and the bulge. The high halo fraction is mainly due to the observational advantages with regard to stars in the halo. The halo is on average metal-poor, and it is sparsely populated, allowing for clear lines of sight toward the stars, compared to, e.g., the dense bulge region.

*Bulge:* recent efforts to find metal-poor stars in the bulge have added 45 stars to the general population of metal-poor stars.

*Classical dwarf galaxies:* 53 stars in JINAbase are located in the classical dwarf galaxies such as Draco, Ursa Minor, Carina, Sextans, Leo I, Sculptor, and Fornax.

*Ultra-faint dwarf galaxies:* there are 43 stars identified as members of ultra-faint dwarf galaxies. This includes the following galaxies, Segue 1 and 2, Reticulum II, Coma Berenices, Canes Venatici II, Leo IV, Ursa Major II, Bootes I and II, and Hercules.

*Position.* Coordinates' right ascension and declination (J2000) are collected from SIMBAD, following the identification of the star in the SIMBAD database.

*Velocity.* Available radial velocity measurements and references collected from SIMBAD. No vetting has been applied; they might not be the latest values or could be based on medium-resolution spectroscopy rather than high-resolution spectroscopy. The corresponding references should be consulted for more information.

*Magnitudes.* Any of the available magnitudes (*U, B, V, R, I, J, H, K*) are collected from SIMBAD.

*Stellar parameters.* Effective temperature, surface gravity, model metallicity, and microturbulence are collected from the same references as the abundances.

*Chemical abundances.* $\log \epsilon (X)$ abundances, for elements from Li to U, when available. Abundances for some elements with two ionization states are also included. NLTE label: as more studies are reporting NLTE chemical abundances and/or stellar parameters, we have included a label in JINAbase to indicate if a star was studied using NLTE. The author can assign this NLTE label to specify NLTE abundances or NLTE stellar parameters or both.

### 2.4. Comments on the Element Signature Labels

As described above, labels are assigned to stars with characteristic abundance signatures for an easy selection of these stars to test nucleosynthesis and chemical evolution models. Here we provide additional comments on these groups of stars. However, we note that all of the labels are completely optional for users to make use of. Also, these labels cannot replace a thorough understanding of the abundance data and their pedigree.

*CEMP stars.* When constructing a sample of carbon-rich stars for any model comparisons, the scientific question drives sample selection. For studies of the carbon enrichment of early gas, *s*-process stars, *i*-process stars, and *r* + *s* stars have to be strictly excluded (by deselecting the relevant boxes) as the carbon abundances of these stars are not representative of the stars' birth environment and instead in all likelihood is from mass transfer events from binary companion stars. On the contrary, for studies, e.g., related to the dredge up of nucleosynthesis products, or mass transfer processes, or early asymptotic giant branch (AGB) carbon production, then a sample of *s*-process or *i*-process stars needs to be chosen.

Overall, 25% of observed extremely metal-poor stars with [Fe/H] $\leqslant -3.0$ are carbon-rich with [C/Fe] $> 0.7$. However, as stars are ascending the giant branch, carbon gets converted to nitrogen. Observed carbon abundances thus do not necessarily reflect the composition of the birth gas cloud, i.e., they show signs of self-enrichment in C and N. Placco et al. (2014c) calculated such corrections using stellar evolution models. This enables the birth composition of these stars to be studied. This then also allows the true frequency of CEMP stars to be determined upon exclusion of *s*-process, *i*-process, and *r* + *s* stars whose large carbon abundances are not arising from the birth cloud but from mass transfer events which mask any contribution from self-enrichment along the giant branch. Knowing the true frequency can assist in better understanding the many origins of carbon, which remain to be understood in detail as sources seem ubiquitous. Options include different types of early supernovae that pre-enrich the gas from which the extremely metal-poor stars form. This is of particular importance, as the fraction of CEMP stars steadily increases with decreasing metallicity, from 25% at [Fe/H] $\leqslant -3.0$ up to 100% at the lowest [Fe/H].

*CEMP-no stars.* These are CEMP stars that show no overabundance (i.e., "normal," subsolar levels) in neutron-capture elements, as measured by barium. Most CEMP stars with [Fe/H] $< -3.0$ are CEMP-no stars, as *s*-process stars begin to rise only at [Fe/H] $> -2.6$ (Simmerer et al. 2004). The lack of neutron-capture element enhancements at the lowest metallicities remains to be understood but observationally establishing their frequency will help address any underlying enrichment processes.

*r-process.* About 2.5% of metal-poor stars with [Fe/H] $< -2.5$ show a strong enhancement (*r*-II stars) in *r*-process elements (Barklem et al. 2005). Another 10% show a mild enhancement (*r*-I stars). Their chemical signature for heavy elements above barium follows the scaled solar *r*-process pattern.[6] Among light neutron-capture elements, there are variations with respect to the scaled solar pattern, though. The reasons for this are largely unknown but include possibilities for multiple *r*-processes production sites (Hill et al. 2002). Presumably, these stars formed from gas that was enriched in these elements by a neutron star merger (Ji et al. 2016b) or an unusual jet-drive supernova (Winteler et al. 2012) in the early universe.

*Limited r-process stars.* Core-collapse supernovae may contribute light neutron-capture elements (from strontium up

---

[6] The scaled solar *r*-process pattern is obtained from subtracting the theoretically well-understood *s*-process component from the total solar abundances. It is thus a derived product, not a measurement.

to barium) in a limited *r*-process (Wanajo 2013) that is driven by a limited flux of neutrons (Frebel 2018). Neutrino-driven winds from millisecond protomagnetars during other types of supernova explosions (Vlasov et al. 2017) might in turn contribute both light and heavy neutron-capture elements. Alternatively, neutron star mergers might have components, e.g., neutrino-driven winds, that produce primarily light neutron-capture elements. HD122563 is a prime example for what can be considered a limited-*r* star (Honda et al. 2006). Currently about 40 stars in JINAbase appear to satisfy the limited-*r* criteria.

*s-process stars.* Some metal-poor stars display large amounts of neutron-capture elements associated with the *s*-process in their spectra. These stars are thought to be in binary systems. A former primary AGB companion transferred mass to the (now observed) lower mass companion, enriching it with *s*-process elements as well as large amounts of carbon that were initially produced in the AGB star (Karakas 2010; Bisterzo et al. 2012). This is why large amounts of carbon (e.g., [C/Fe] > 1.0) are always present in these stars. Today, only the lower mass secondary star is observed. It should be noted here that AGB stars are numerous throughout the universe, and thus significantly enrich their surrounding ISM with carbon and *s*-process elements through their stellar winds in their own right. This leads to significant contributions to the global chemical evolution, and the carbon and *s*-process element enrichment of the gas from which all subsequent (metal-poor) stars formed. Such global enrichment appears to occur only from [Fe/H] > −2.6 (Simmerer et al. 2004), due to the delay time needed for the very first lower mass stars to become the first AGB stars in the universe. This enrichment channel has to be included in chemical evolution models, whereas *s*-process metal-poor stars that receive their chemical signature from a mass transfer event provide tests for AGB nucleosynthesis, carbon production, and binary systems.

*r + s stars.* So far, only one star has been found with a neutron-capture element abundance pattern that can plausibly be explained with a combination of the *r*- and *s*-process patterns (Gull et al. 2018). The star likely formed from gas enriched by an *r*-process and then later received *s*-process material from a companion in a binary system. Future searches will hopefully uncover more of these stars.

*i-process stars.* Some metal-poor stars show strong enhancements in neutron-capture elements that do not match either the scaled solar *s*- or *r*-process. These stars were termed "*r + s*" stars because it initially looked like a combination of these two processes would explain the observations. But many studies showed that another explanation is needed for these stars (Jonsell et al. 2006). Recent studies have then invoked the "intermediate" (*i*-)process that may also occur in AGB stars (Hampel et al. 2016; Denissenkov et al. 2017). While more studies are needed to fully explain these observed patterns (F. Herwig et al. 2018, in preparation), it seems that the *i*-process is likely responsible for these neutron-capture signatures. All *i*-process metal-poor stars would then be in binary systems that received enriched material from their AGB companion.

In closing, we note that carbon enhancement naturally goes along with most of these signatures. An exception might be *r*-process stars since any carbon enhancement would exclusively come from an (extrinsic) enrichment of the gas from which they formed, rather than any (generic) binary companion. Nevertheless, a few carbon-enhanced *r*-process stars are known, e.g., CS 22892-052 (Sneden et al. 2003), and as more are discovered their nature will be revealed.

### 2.5. Frequencies of Stars with Particular Element Signatures

Observationally establishing the frequencies of groups of stars that show a common elemental signature helps to gain a deeper understanding of their astrophysical origin scenario. It also assists theoretical modeling to learn more about the associated nucleosynthesis processes responsible for the elements that are observed in metal-poor stars. Frequencies have previously been assessed by e.g., Rossi et al. (1999), Frebel et al. (2006a), Lucatello et al. (2006), Placco et al. (2014c), and others for carbon-enhanced stars from the literature, or Barklem et al. (2005), and Hansen et al. (2018) for *r*-process stars based on their respective samples.

In Table 2, we list raw numbers and frequencies of halo stars for three different metallicity ranges, as extracted from JINAbase. As classifications may change in the future and stars' elemental signatures are assessed in more detail, these frequencies are likely going to change somewhat. Nevertheless, for now they provide a useful census of the body of metal-poor halo stars. Before discussing various comments with regard to the selections, we highlight that, overall, the results are in line with those of previous studies. Specifically, we find that a total of 19% of metal-poor stars with [Fe/H] < −2.0 have a particular neutron-capture element signature. Below [Fe/H] = −3.0, this drops to 10%, showcasing that the range of −3.0 < [Fe/H] < −2.0 is the richest range for studying neutron-capture nucleosynthesis with metal-poor stars. Adding carbon enhancement ([C/Fe] > 0.7) as another chemical signature that metal-poor stars might display, the rate of stars with [Fe/H] < −2.0 that display a particular elemental signature is 32%. Given the propensity for carbon enhancement at low metallicity, 42% of stars with [Fe/H] < −3.0 show a signature that sets them apart from ordinary halo metal-poor stars. This summarizes that "normality" among metal-poor stars in terms of their elemental abundance patterns is actually limited to about half of the stars only at [Fe/H] < −3.0, and two-thirds for stars with [Fe/H] < −2.0, more generally.

**Table 2**
Frequencies of Metal-poor Halo Stars that Adhere to the Element Signature Criteria Given in Section 2.3

| Label | −2.5 < [Fe/H] ⩽ −2 | | −3 < [Fe/H] ⩽ −2.5 | | [Fe/H] ⩽ −3 | | Total freq |
|---|---|---|---|---|---|---|---|
| | N | freq | N | freq | N | freq | |
| *r*-I | 41 | 14% | 54 | 10% | 18 | 4% | 9% |
| *r*-II | 4 | 1% | 17 | 3% | 7 | 2% | 2.3% |
| *r*-lim | 8 | 3% | 21 | 4% | 13 | 3% | 3.5% |
| *r + s* | 1 | 0.3% | 0 | 0% | 0 | 0% | 0.1% |
| *s* | 13 | 4% | 10 | 2% | 1 | 0.2% | 2% |
| *i* | 11 | 4% | 14 | 3% | 2 | 0.5% | 2.2% |
| $N_{\text{n-cap. sign.}}$ | 78 | 27% | 116 | 23% | 41 | 10% | 19% |
| $N_{\text{total}}$ | 292 | | 506 | | 415 | | 1213 |
| CEMP-no[a] | | 3% | | 16% | | 32% | 13% |
| $N_{\text{CEMP+n-cap.}}$ | | 30% | | 39% | | 42% | 32% |

**Notes.** Only stars with priority 1 are included here to give a realistic estimate of the frequency for each subclass.
[a] CEMP frequencies taken from Placco et al. (2014c) because they are corrected for the evolutionary status of the stars.

In the following, we comment on how these frequencies were obtained from JINAbase. First of all, the body of data contains results from papers up to mid 2016. More recently, e.g., papers reporting the discoveries of $r$-process stars have been published (e.g., Hansen et al. 2018) but those are not included in this study to not bias the sample in a particular way. Future updates to JINAbase will of course include those and other more recent papers.

As for the selection of $r$-I and $r$-II stars, we used the given selection criteria of $0.3 \leqslant [Eu/Fe] \leqslant +1.0$ and $[Ba/Eu] < 0.0$, and $[Eu/Fe] > +1.0$ and $[Ba/Eu] < 0.0$, respectively (see Section 2.3). Ideally, abundances for elements beyond Ba and Eu are available to ensure that the main $r$-process pattern is indeed observed in these stars. Future selections may thus include additional elements to test for the existence of the pattern already during the selection. As for the selection of limited $r$-process stars, we opted not to employ the $[Sr/Eu]$ criterion but only used $[Eu/Fe] < +0.3$ and $[Sr/Ba] > +0.5$ (see Section 2.3). The reason is that Eu has not always been measured or has no useful upper limit reported. Future analyses can better address the need for a Eu abundance/upper limit with this additional $[Sr/Eu] > 0$ criterion, as it will lead to a more precise selection of limited $r$-process stars. Overall, we thus caution that the $r$-lim frequencies should strictly be taken as lower limits due to the common non-availability of Eu abundances which precludes the identification of an underlying abundance signature.

As for the selection of $s$-process stars, we opted not to employ the $[Ba/Pb]$ criterion but only the traditional $[Ba/Fe] > +1.0$ and $[Ba/Eu] > +0.5$. Pb is not measured in all $s$-process stars, thus preventing their proper identification. Future analyses can better address the need for a Pb abundance/upper limit with this additional $[Ba/Pb] > -1.5$ criterion. As for the selection of $i$-process stars, we opted to identify them based on literature results rather than the given criteria in Section 2.3. While the sample identified might be (currently) incomplete, the abundance criteria could not sufficiently reproduce the $i$-process stars because not enough neutron-capture elements, especially Hf and Ir, are measured in all these stars. Future analyses can better address the need for Hf and Ir abundances/upper limits so that both the $0.0 < [La/Eu] < 0.6$ and $[Hf/Ir] \sim 1.0$ criteria can be meaningfully applied to select these stars. Another complication lies in the apparent similarity of $s$-process and $i$-process stars. To ensure a good $s$-process star selection, we subtracted the hand-selected $i$-process stars from the $s$-process list since many were selected as $s$-process stars when only applying the $[La/Eu]$ criterion.

In order to select the one known $r + s$ star to illustrate the newly developed selection criteria and extremely small frequency, we added the recent result of Gull et al. (2018). This is the only recent paper included in the frequency analysis.

For the selection of CEMP-no stars, we took frequencies from Placco et al. (2014c) who correct carbon abundances for the evolutionary status of the star. Their results are also based on an earlier version of the JINAbase compilation (Frebel 2010) so that the underlying data sample is relatively similar and hence comparable. To obtain the final combined frequencies, we simply added the frequencies from the neutron-capture signatures to those taken from Placco et al. for the respective metallicity range. This addition is feasible since there is no overlap expected between CEMP-no stars and stars in the

neutron-capture signature categories besides less than half a dozen CEMP-$r$ stars which we regard negligible.

In closing, we emphasize here again that the JINAbase labels are assigned according to these more simplified criteria. Going forward, however, and keeping those improved (albeit more difficult to adhere to) criteria in mind, abundance determinations should aim to measure these additional elements so that stars can be more accurately selected.

### 2.6. The JINAbase Web Application

The web app is divided into tabs. A navigation bar includes the four main tabs: Home, Query/Plot, Search, and References. Additionally, the navigation bar includes a frequently asked questions tab, a short guide to using JINAbase, and the option for users to log in or register. Users can register to gain access to the web app's advanced functionalities. The registered user can upload data to the database, edit pre-existing data (see also Section 2.8), and be able to download the entire database content as a csv file. The database is free to use; however, the registration step is set to enable us to reject spam, keep track of changes and uploads to the database, and collect statistics on the usage of the database. We added this feature to facilitate maintaining the database; this way it is a community effort. The Home tab includes a brief general description of the tabs and lists recent updates from the developer. It also includes information for how to cite the database, as well as contact information to report bugs and suggestions for further improvement.

The Query/Plot tab interface is divided into several panels guiding the user through the steps needed to choose a particular sample of stars. A screenshot of the Query/Plot tab content is shown in Figures 2 and 3. The first panel has the options to select the main abundances/stellar parameters to query or plot as well as which solar abundances to use if needed. The selection is divided into $x$- and $y$-axis data, with a numerator and denominator selection for each. These options form the base for any selected sample. For ease of plotting, empty "From" and "To" boxes plot all available data. Another option is to define either the "From" or "To" box alone, leaving the other box empty to set no limit. The user can also add additional selection criteria to customize the sample using other chemical elements or stellar parameters ($T_{eff}$, [Fe/H], $\log g$, $v_t$); this feature is available in the second panel. Up to two extra criteria can be added. This way, the user can choose, e.g., user-defined carbon-enhanced stars or select only stars in a specific effective temperature range.

Next, there are a number of choices the user can make to further refine the sample selection. One can choose from locations of the stars (Milky Way halo, bulge, classical dwarfs, and ultra-faint dwarfs), stellar evolutionary status (red giants, subgiants, main-sequence (near) TO, and horizontal branch stars), and pre-defined characteristic element signatures (ordinary stars with no special element signatures; $r$-I, $r$-II and $r$-limited $r$-process, $s$-process, $i$-process, $r + s$-process stars; as well as CEMP and CEMP-no stars). The selection criteria for these groups of stars are described in Section 2.3 and further comments are given in Section 2.4.

At this point, the sample of stars desired is defined. Then, all or any set of references can be selected to query. Selecting at least one reference is required to query the database. All or individual references can be selected from the provided table or

**Figure 2.** A screenshot of the Query/Plot tab from the web app. This figure shows the panels displayed in the top half of the tab. These panels guide the user through selecting their sample of metal-poor stars. The remaining panels are shown in Figure 3.

a first author's last name (separated by a comma if more than one) and/or a year range can be entered in the search boxes to query the list of references included in JINAbase. After the references are selected, the user can either plot the selected sample to explore it using an interactive plot or display it as table. We recommend exploring the sample through the plot before generating the output table.

Finally, there are options for adding supplementary information to the output table to download. First, when attempting to extract data for a specific sample, the user can add up to three extra elements to be included in the output table; otherwise, just the two entries selected at the very top for the *x*- and *y*-axes will be outputted. Alternatively, *all* available abundances for the selected sample can be outputted when ticking the respective box.

In addition, the user can specify additional information. This includes literature stellar parameters (which are used, e.g., above to calculate the stellar evolutionary status), additional JINAbase information (JINAbase ID, JINAbase priority key (based on the study with the largest number of measured chemical abundances), literature star name), and SIMBAD information (SIMBAD name, coordinates R.A. and decl., different magnitudes, and radial velocity information).

Users can search JINAbase for a star (list of stars) using the Search tab. A screenshot of the Search tab content is shown in Figure 4. The content of the Search page is divided into three

main tabs. There are three main options for searching in JINAbase: (1) using the literature or SIMBAD identifier or by R.A. and decl. coordinates given a search radius, (2) searching by reference(s) using the references table, and (3) searching using JINAbase's ID, if known beforehand (e.g., from the Query tab). These three options are independent, hence they are displayed in separate tabs.

There are two options for viewing the result of a search, either by plotting the chemical abundances (specifying the desired format) versus the atomic number or as a table. The format and atomic number range of the chemical abundances can be specified from the second panel, along with the solar abundances to use if needed. The result table includes, by default, the chemical abundances of the star(s). The user can add extra information to the table using the given options in the last panel, just like in the Query/Plot tab. The user can then save the table as a simple ascii file.

The References tab includes a table with all the literature included in the database. Links to the papers and the bibtex entries on ADS are included, as well as the number of stars per study. Each entry in the output tables is assigned the corresponding reference code on this page. This enables easy referencing of all original papers after constructing custom samples. Extra options are added to the navigation bar depending on the role assigned to the logged in user.

**Figure 3.** The second half of the Query/Plot tab from the web app.

### 2.7. How to Extract JINAbase Content—Examples

We now comment on and describe several examples for common queries and questions.

*How to extract stars below/above a certain [Fe/H] value.* Plotting (and downloading) stars below/above a certain value is one of the most common requests. In JINAbase, there are two ways to achieve this.

(1) Select stars using the elements iron and hydrogen to impose an [Fe/H]-based selection. This selects on the [Fe/H] abundances obtained in each analysis. For the

**Figure 4.** A screenshot of the Search tab from the web app.

other axis, choose any desired element. Note that only stars that have this element abundance available will be selected. Alternatively, one of the stellar parameters could be chosen from the dropdown menu for the other axis as the "numerator element" while leaving the "denominator element" empty (or ignoring it). Stellar parameters are available for all stars. Next, specify one, both, or none of the From and To values. Leaving the box blank means that no limit is placed on the data, i.e., everything will be included. Make sure no additional abundance criteria are selected from the panel titled "Need more abundances or stellar parameter criteria?"

(2) A sample of stars below a certain [Fe/H] can be selected by adding a user-defined criterion based on the selection of iron and hydrogen. This criterion is applied in addition

to the initial options selected for the *x*- and *y*-axes. Only stars will be included in the query that adhere to the *x*- and *y*-axis selection (within their specified range) *and* to the specified [Fe/H] cut.

*How to include additional elements in the output table.* To include all the abundances of all the stars in the output table, tick the box at the bottom of the page to Add all elements, specifying the preferred format of the abundances. Then use Plot abundances to plot the queried data or Show data table to generate the output table. The data table can then be downloaded (in user-selected format). (Do not forget to also choose solar abundances, location of stars, evolutionary phases, inclusion of upper limits, specific element signatures, etc., as desired.)

10

*How to plot $T_{eff}$ versus log g.* In the Query/Plot tab, select $T_{\rm eff}$ for the *x*-axis and log *g* for the *y*-axis (as the "numerator elements" and leaving the "denominator elements" empty or ignoring them). Switch the From and To values to force reverse plotting of the axes to obtain a Hertzsprung–Russell diagram plot. Add an [Fe/H] or other abundance constraint by choosing an Add criterion, if desired.

What additional data products are available for download? Abundances [X/H] and [X/Fe] are calculated with user-chosen solar abundances. They are used for plotting and can also be downloaded.

*How to download the entire JINAbase content.* The entire content of JINAbase can be downloaded as a csv file. After registering with the database, the user gains access to the internal pages of the web app. Once logged in, the user can move to the Data table tab from the navigation bar. An option to export the entire content of the database is available at the top of the page.

### 2.8. Using JINAbase in Your Research Now and in the Future

The goal for constructing JINAbase has been to provide easy access to the chemical abundance data of metal-poor stars. While this is largely achieved with the web-based queryable tool, we have also created a black box in the sense that analysis details are not stored but will in all likelihood be different for every study included. This means that there is no substitute for checking, and citing, the original papers. JINAbase links to all papers for easy access and also provides bibtex entries. If you used JINAbase for your work, kindly cite this work as well.

Long term, JINAbase will be a "living" database that will be continuously updated as new results become available. Results from new (or currently missing) papers can be uploaded by authors themselves after signing up as contributors. This will assist in keeping the database content up to date. Registration and login links can be found in the navigation bar at the JINAbase website. Uploading instructions are provided upon logging in. Alternatively, the authors of this paper can be notified about large data sets to include.

There are also possibilities to later on include abundance data for, e.g., stars in globular clusters and metal-rich stars from various populations, and secondary information such as distances and kinematics from *Gaia*, when available. Large survey samples reporting chemical abundances from, e.g., APOGEE[7] (García Pérez et al. 2016) would also be helpful to add, but a workaround is needed for this to work smoothly with the web app. Currently, we estimate that no more than around 10,000 entries can be accommodated without very significantly delaying the queries.

### 3. Assessing Systematic Difference in Stellar Parameters and Abundances between Multiple Literature Studies Using Three Metal-poor Stars

Data collected in JINAbase can easily be used to conduct statistical studies on various abundances of metal-poor stars. This benefits observers as well as theorists in, e.g., assistance with planning new observations or maximizing the value that the available data provides. There are a few stars that are regularly used as reference metal-poor stars in abundance studies. In addition, there are many stars that have been

---

7 http://www.sdss.org/dr12/irspec/spectro_data/

---

**Table 3**
Variations in Literature Stellar Parameters for Three Well-studied Metal-poor Stars

|  | Mean | Median | Std | Min | Max |
|---|---|---|---|---|---|
| HD122563 | | | | | |
| $T_{\rm eff}$ | 4568 | 4600 | 65 | 4425 | 4650 |
| log *g* | 1.12 | 1.10 | 0.30 | 0.50 | 1.50 |
| [Fe/H] | −2.77 | −2.77 | 0.13 | −3.06 | −2.51 |
| $v_{\rm mic}$ | 2.20 | 2.20 | 0.31 | 1.70 | 2.90 |
| HD140283 | | | | | |
| $T_{\rm eff}$ | 5737 | 5750 | 50 | 5630 | 5830 |
| log *g* | 3.58 | 3.66 | 0.16 | 3.20 | 3.73 |
| [Fe/H] | −2.52 | −2.54 | 0.11 | −2.71 | −2.26 |
| $v_{\rm mic}$ | 1.46 | 1.40 | 0.48 | 0.75 | 3.00 |
| G64−12 | | | | | |
| $T_{\rm eff}$ | 6313 | 6333 | 173 | 6030 | 6550 |
| log *g* | 4.17 | 4.20 | 0.35 | 3.58 | 4.68 |
| [Fe/H] | −3.31 | −3.27 | 0.14 | −3.58 | −3.10 |
| $v_{\rm mic}$ | 1.67 | 1.50 | 0.34 | 1.20 | 2.30 |

---

analyzed by multiple groups. In total, JINAbase contains 437 stars with multiple entries. Each study naturally reports slightly different stellar parameters and chemical abundances due to the different methods and tools employed. We use this to aid in identifying systematic differences between different studies. In this section, we provide general uncertainties relating to metal-poor stars that can be used in theoretical models when using data from JINAbase.

We now assess these systematic differences for the three most well-studied metal-poor stars. HD122563, a cool red giant, has 28 entries in JINAbase, HD140283, a subgiant, has 21 entries, and G64−12, a main-sequence star, has 16 entries. Furthermore, the evolutionary status of the stars broadly explains the number of reported abundances per study. The red giant star with the intrinsically strongest lines has the largest number of individually reported abundances by all studies. On the contrary, for the other two much warmer stars with intrinsically weaker lines, a number of chemical elements are reported only in one to two studies.

*HD122563.* In terms of stellar parameters, the effective temperature shows a range of 225 K with a median value of 4600 K. The surface gravity has a range of 1 dex with a median of 1.1. The metallicity spans a range of 0.5 dex with a median of [Fe/H] = −2.71. The microturbulence spreads 1.2 km s$^{-1}$ with a median of 2.2 km s$^{-1}$. Table 3 gives more details on the spreads and values in stellar parameters. Figure 5 (top panel) shows the various log $\epsilon$ (X) abundances reported in the literature for HD122563. In Figure 6 (top row of both sets of panels), we show the standard deviations of the log $\epsilon$ (X) and [X/Fe] abundance measurements available for each element. Those vary between 1 and 28 measurements. We also list the number of measurements per element to show the significance of the standard deviation. Upper limits are not included in the standard deviation calculation. The median standard deviation between studies for HD122563 is 0.16 dex. For elements with only one abundance measurement, we adopt the median standard deviation, for plotting purposes.
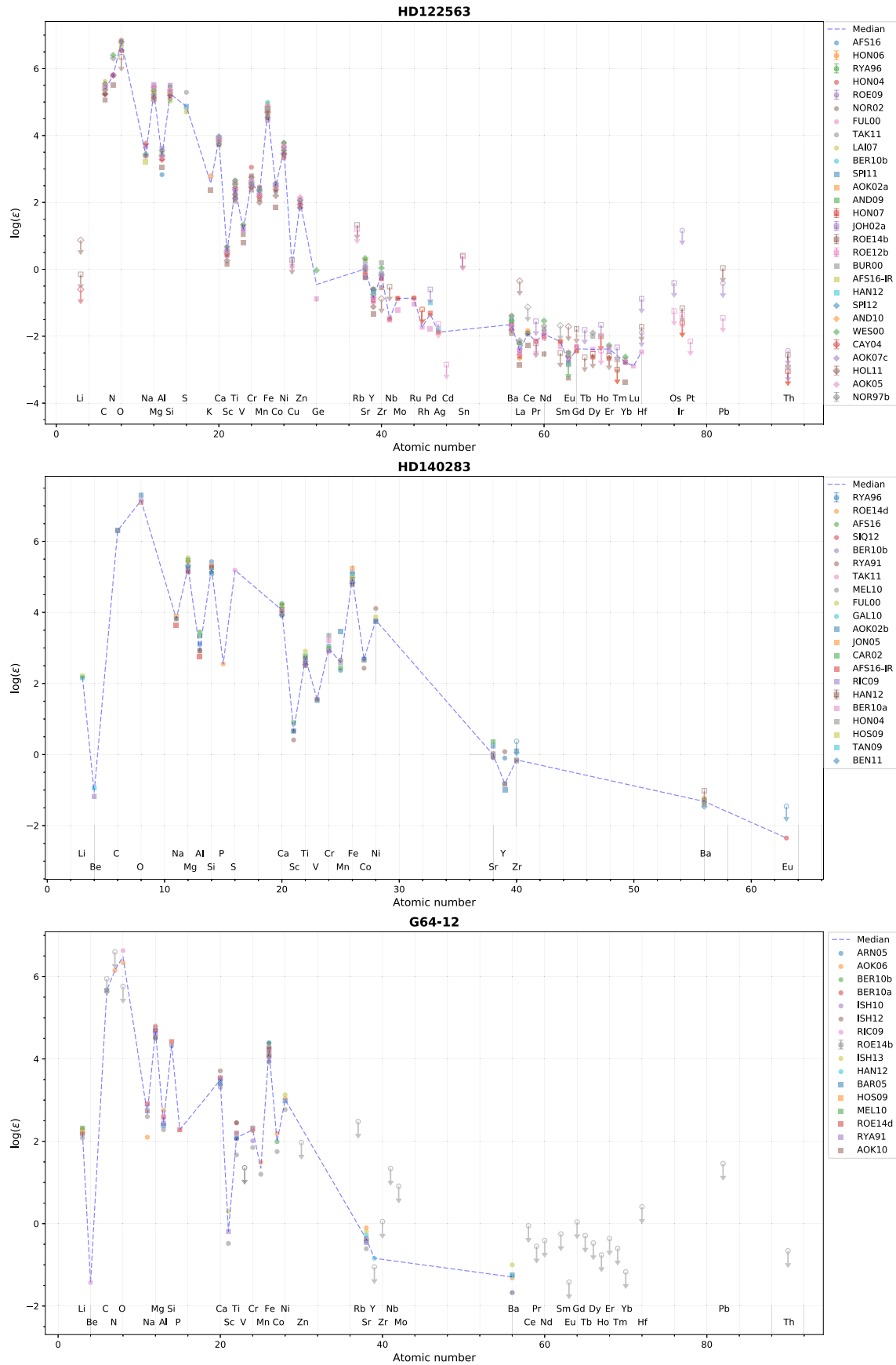
**Figure 5.** Chemical abundances $\log(\epsilon)$ of available studies in the literature as a function of atomic number for three well-studied metal-poor stars. Results from 28 studies are shown for HD122563 (top), 21 studies for HD140283 (middle), and 16 studies for G64−12 (bottom). The median for each element is shown as the blue dotted line; upper limits are not included in median calculation. The differences in measurements per chemical element can be seen from the scatter for each element. References are labeled.
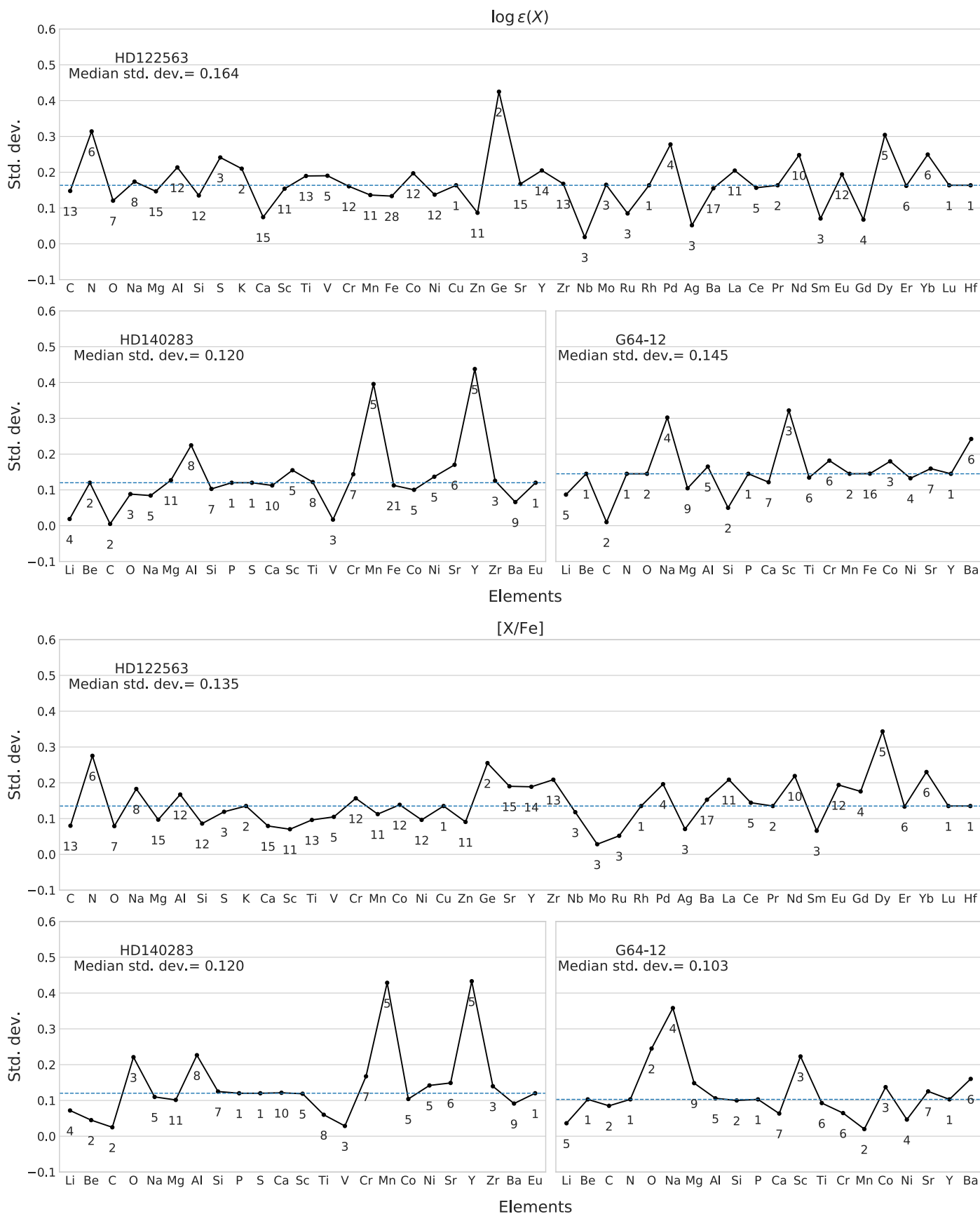
**Figure 6.** Standard deviation of log ϵ (X) abundances (top set of panels) and [X/Fe] abundances (bottom set of panels) per element from all of the different measurements for HD122563, HD140283, and G64–12. Upper limit measurements are not included. The blue dashed line shows the median standard deviation from all of the elements with more than one measurement. For elements with only one measurement, we used the median standard deviation. The number of measurements for each element is shown below the data points.

*HD140283.* In terms of stellar parameters, the effective temperature shows a range of 200 K with a median value of 5750 K. The surface gravity has a range of 0.5 dex with a median of 3.7. The metallicity spans a range of 0.5 dex with a median of $-2.5$ dex. The microturbulence spreads a huge 2.25 km s$^{-1}$ with a median of 1.4 km s$^{-1}$. Table 3 gives more details on the spreads and values of the stellar parameters.

Figure 5 (middle panel) shows the various $\log \epsilon$ (X) abundances reported in the literature for HD140283. In Figure 6 (bottom left plots in each panel set), we show the standard deviations of the $\log \epsilon$ (X) and [X/Fe] abundance measurements available for each element. Those vary between 1 and 21 measurements. We also list the number of measurements per element to show the significance of the standard deviation and upper limits are not included. The median standard deviation for HD140283 is 0.12 dex.

*G64−12.* In terms of stellar parameters, the effective temperature shows a range of 520 K with a median value of 6333 K. The surface gravity has a range of 0.9 dex with a median of 4.2. The metallicity spans a range of 0.4 dex with a median of $-3.3$. Table 3 gives more details on the spreads and values of the stellar parameters. The microturbulence spreads 1.1 km s$^{-1}$ with a median of 1.5 km s$^{-1}$. Given the fact that G64−12 is extremely metal-poor and fairly warm, only few Fe lines are available. This could explain why the literature values agree to only within $\sim$500 K if a significant number of these studies used spectroscopic techniques to determine the temperature.

Figure 5 (bottom panel) shows the various $\log \epsilon$ (X) abundances reported in the literature for G64−12. In Figure 6 (bottom0right plots in each set of panels), we show the standard deviations of the $\log \epsilon$ (X) and [X/Fe] abundance measurements (and numbers of measurements) available for each element. Those vary between 1 and 16 measurements. Upper limits are not included. Typical systematic uncertainties between studies for G64−12 are $\sim$0.15 dex based on the median standard deviation.

Despite the many different studies, the effective temperatures are all within $\sim$200 K for HD122563 and HD140283. Standard deviations are a very reasonable 50–60 K given that uncertainties of 200 K are typical across different analysis techniques. For surface gravity, disagreement is large for HD122563 and G64−12, on the order of $\sim$1 dex, and moderate for HD140283 (0.5 dex). Gravity is notoriously difficult to determine (e.g., Jofré et al. 2014; Heiter et al. 2015), which is reflected in these numbers. Metallicity [Fe/H] varies moderately, at the 0.4–0.5 dex level, and likely mainly a result of the uncertainties in the effective temperatures and microturbulence. With differences of more than 1 km s$^{-1}$, microtubulences wildly disagree between studies, which is somewhat concerning.

What is very encouraging, though, is the overall good agreement between all available studies when it comes to the chemical abundance measurements. Average standard deviations between studies for all elements are around 0.15–0.20 dex. These can be regarded as robust general systematic uncertainties on elemental abundances and should be used in various model comparisons. They also agree with typical standard deviations of iron abundances based on line-by-line measurements.

Broadly speaking, typical systematic uncertainties in the analysis of metal-poor stars arising from different analysis methods are thus

$\sigma(T_{\rm eff}) = 65$ K, $\sigma(\log g) = 0.3$ dex, $\sigma(v_{\rm mic}) = 0.34$ km s$^{-1}$, $\sigma([{\rm Fe/H}]) = 0.13$ dex, $\sigma(\log \epsilon$ (X)$) = 0.15$ dex, and $\sigma([{\rm X/Fe}]) = 0.12$ dex.

These values are the medians of the standard deviation values; see also Table 3 and Figure 6.

To put these numbers in perspective, Smiljanic et al. (2014) present a statistical analysis of $\sim$1300 FGK-type stars. Their approach is similar to what we tested above. The stars were analyzed by different groups following different methodologies. They then present systematic uncertainties for the stellar parameters and individual chemical abundances for 24 elements. For the effective temperature, systematic differences are 50–100 K; for $\log g$, they are 0.1–0.25 dex, and 0.05–0.1 dex for [Fe/H]. Typical dispersions of the individual chemical abundances range from 0.10 to 0.20 dex. The median uncertainties quoted in Smiljanic et al. (2014) are

$\sigma(T_{\rm eff}) = 55$ K, $\sigma(\log g) = 0.13$ dex, and $\sigma([{\rm Fe/H}]) = 0.07$ dex.

The result we find for effective temperature is surprisingly similar to that reported in Smiljanic et al. (2014). For $\log g$ and [Fe/H], the literature sample has about twice the uncertainties reported in Smiljanic et al. (2014). This can be easily understood given the broad range of analyses, model input choices, and spectra used across all literature studies.

## 4. Guide for Choosing Element Abundance Samples of Metal-poor Stars for Model Comparisons

Models of nucleosynthesis and chemical evolution generally rely on comparisons with abundance data from metal-poor or other stars. JINAbase offers a straightforward way to collect suitable samples for such comparisons, given that the body of low-metallicity stellar spectroscopic data has significantly grown in recent years. A common pitfall with such a compilation is that analysis and other details specific to each study are essentially lost, as only the "bare bones" numbers are propagated. It can thus be challenging, and perhaps even misleading, to choose a suitable sample for model comparisons. Given that the onus is on the observer to provide suitable data samples to theorists for model comparisons, we choose here to provide a general guide to common issues regarding various elemental abundances. The main purpose of this section is to introduce the interested novice or non-spectroscopists (e.g., students, theorists) to a minimum amount of community wisdom regarding the analysis and interpretation of spectroscopic abundance data of metal-poor stars with the aim to assist them in making informed choices when selecting comparison samples. We note that the following discussion pertains to metal-poor stars (with [Fe/H] $\lesssim -2.0$ or so) and does not necessarily translate to more metal-rich stars or solar-metallicity stars.

In the following, we thus comment on various elements, their general availability in abundance studies, usability for model comparisons, caveats about abundance determinations, and uncertainties. This includes the good, the bad, and the ugly from the trenches of the dark art of spectroscopy using mainly optical (and some near-UV and UV) high-resolution spectra.

Near-infrared studies hold a different set of secrets. We critically stress here that this guide will never be 100% complete, and it does in no way replace consulting original papers for the many details of each study, and even for individual stars.

It should also be noted that many improvements regarding the details of abundance analyses (e.g., NLTE, 3D calculations) have been made in the last few years (Gallagher et al. 2017; Nordlander et al. 2017). However, these are not yet available for many (most) stars and their abundances, and whatever has been collected from the literature has likely not (yet) benefited from these advances. We thus focus on common issues that pertain to the majority of elemental abundance measurements in the literature. This includes, unfortunately, LTE and some NLTE abundances being mixed without any particular labeling, although we have added options for flagging LTE or NLTE abundances as such for future inclusions of data sets to JINAbase.

Information on isotopic abundances are not discussed further, mainly due to the fact that hardly any are available and usually they have large uncertainties. Elements for which isotopic abundances have been determined in very few stars are Mg, Ba, and Eu. One exception is carbon isotope ratios that are easier to determine and have been measured in many metal-poor stars. However, JINAbase has not recorded isotopic abundances.

Finally, uncertainties are further discussed in Section 3 but we note here that for bright halo stars for which high-quality spectra can be obtained, the uncertainties will naturally be much smaller than for dwarf galaxy stars for which barely useful data can just be obtained with the current biggest telescopes.

### 4.1. Lithium

As stars evolve from the main sequence to the subgiant branch to the red giant branch, lithium gets increasingly destroyed. The surface abundance thus decreases. With the convection zone deepening, lithium from the outermost (observable) layers is transported into hotter, inner regions, where it captures $\alpha$-particles, only to then fall apart to beryllium. Hence, lithium can only be detected in warmer stars (up to about the middle of the subgiant branch) that still have thin convection zones. The corresponding decline of lithium abundance with evolutionary status is well established.

Near-main-sequence TO stars (with no expected surface depletion) show abundances in accordance with what has been termed the "Spite plateau," $A(\mathrm{Li}) \sim 2.3$. (The nomenclature for lithium abundances is different from that of other elements. While other elements are usually given as [X/Fe], lithium is given in the $\log \epsilon(\mathrm{X})$ number density format although relabeled as $A(\mathrm{Li})$, with $A$ standing for "Abundance." The reason is that lithium is not produced in fusion like other lighter elements; see more below.) At the lowest Fe abundances, there is currently a debate about stars with abundance lower than the Spite plateau, especially in light of the fact that the Spite Plateau value is already 0.3 dex lower than what is predicted from standard Big Bang nucleosynthesis. Potential lithium depletion mechanisms in stellar atmospheres are poorly understood, which have lead to this being a decade-old problem. Selected 3D and NLTE studies (e.g., Korn et al. 2006; Lind et al. 2013) have provided insight into this problem but could not solve it.

The observed lithium abundances in the most metal-poor stars are thought to reflect the primordial Li abundance since lithium is only made through cosmic rays and spallation processes and not in stars through the standard fusion processes as with all the other lighter elements. Lithium thus does not follow a "chemical evolution" like other elements and should not be used for comparisons with, e.g., supernova yields or chemical evolution models.

An interesting alternative use of lithium is when Li-rich giants are observed. In a small number of red giants, huge overabundances of lithium are found, in stark contrast to what would be expected from their evolutionary status. Indeed, the reason for the enhancement is that for a short phase up on the giant branch, the Cameron-Fowler beryllium transport mechanism is able to flush Li-rich material to the surface. Then, Li overabundances can be observed. Soon after, convection and dredge-up processes will lead to the destruction of lithium again. It remains unclear if this short-lived surface enrichment significantly contributes to the chemical evolution of lithium. It rather provides data to constrain internal stellar evolutionary and mixing processes.

### 4.2. Carbon

Carbon is usually determined from molecular features of CH at 4313 and 4323 Å. In the case of very strong carbon features in the spectrum (due to either a strong carbon enhancement and/or the cool temperature of the star which increases intrinsic line strength), the $C_2$ band at $\sim5130$ Å is also used. It only becomes measurable when the carbon abundance is very high (exact abundances will depend on the temperature of the star, but s-process and i-process stars usually have this occurring). Modeling the line formation of molecules is more complex than that of atomic features. The widespread use of 1D LTE plane-parallel model atmospheres for abundance determination is known to overpredict carbon abundances, especially at low metallicity, compared to 3D hydrodynamically modeled line formation (the temperature structure of the atmosphere is cooler in 3D models, which increases line strength and thus reduces the abundance). While corrections, the so-called 3D effects, are not yet available for larger samples (each star needs to be modeled individually; e.g., Gallagher et al. 2016, 2017), this effect should be kept in mind when comparing with models. Corrections can be as large as 0.7 dex for extremely metal-poor stars (Collet et al. 2006; Nordlander et al. 2017). Also, 1D LTE values can be used since relative abundances and abundance spreads can still be assessed. (NLTE studies have not yet been carried out for hydride molecules.)

Carbon abundances are not just affected by our limited capability to model molecular line formation. A different type of correction that needs to be addressed pertains to the evolutionary status of the star. As the star moves up the red giant branch, carbon gets converted to nitrogen. This results in an in situ change of the carbon abundance of the observed star. This effect technically renders the star useless for stellar archaeology purposes since its carbon abundance no longer reflects the natal cloud, but mixing processes in its interior instead. Fortunately, corrections can be assessed[8] when using as an input the stellar parameters and the 1D LTE carbon abundance. Three-dimensional effects are not accounted for in this procedure.

---

[8]   They can be obtained here: http://www3.nd.edu/~vplacco/carbon-cor.html.

Uncertainties for molecular abundances are usually larger than for other elements, given the spectrum synthesis of an entire band rather than one clean absorption line. The lack of more than two to three bands for any statistics leads to typical uncertainties of about 0.2–0.4 dex, depending on the data quality and strength of the carbon features.

### 4.3. Nitrogen

Nitrogen abundances are affected in similar ways to carbon abundances since they are derived from the molecular NH measure at 3360 Å. Most data do not cover this wavelength regime, which explains why only a few stars have nitrogen measurements. If the N abundance is not enhanced, the chances for detection are decreased as well. Nitrogen is also affected by stellar evolution—it increases as the star moves up the giant branch; see above discussion on carbon. Three-dimensional and NLTE effects equally apply as well, as for carbon. In some cases, nitrogen is obtained from the CN molecular band at 3880 Å. In that case, the nitrogen abundance directly depends on the previously determined carbon abundance. This can lead to additional uncertainties and should be kept in mind. Given that only one feature is available in a region where data quality is usually very low, uncertainties are generally large, around 0.3–0.5 dex.

### 4.4. Oxygen

Oxygen abundance is difficult to determine and should only be used with caution. There are three different oxygen indicators, OH molecular lines in the near-UV around 3100 Å, the forbidden [O] line at 6300 Å, and the O triplet near 7770 Å. Two of the three indicators suffer modeling issues (3D, NLTE) and the third, largely unaffected, one is a weak feature that is not always measurable. Particularly in metal-poor stars, the forbidden [O] line is generally not detected, although it would be the best indicator to use. Only OH and O triplet lines are an option but they depend on the O abundance and evolutionary status (i.e., warm stars will likely not show strong features).

At the lowest iron abundances, only OH lines in the near-UV can be measured, if at all. Data quality is usually very low at these wavelengths, which prevents detection, although stacking spectral regions with lines in it can assist with making a combined detection (Frebel et al. 2006b). OH-based abundances are affected by 3D effects, in the same ways as carbon as described above.

The O triplet can still be measured in some extremely metal-poor stars (with [Fe/H] < −3.0) but the lines are severely affected by NLTE effects. For O triplet lines, strong NLTE effects that affect each line differently further complicate their usage (Amarsi et al. 2016a). Detailed modeling, also in 3D, is required to assess these effects, which is still difficult for larger samples.

When putting together a sample of O measurements, original papers should be consulted to construct a sample based on measurements from the same indicator. Even then, corrections are best taken into account or at least the direction of potential corrections before comparing with model results.

### 4.5. Sodium

Sodium abundances show a large scatter in halo and dwarf galaxy stars (but a well-defined one in globular clusters). This might in part be due to the Na D doublet being easily affected by interstellar Na absorption. In many cases, interstellar absorption is separated from the stellar component by a velocity difference but often no interstellar component is visible. This could be to due no interstellar Na being present or it being aligned with the stellar Na line, thus impacting the stellar Na abundance. Most papers do not report whether or not interstellar absorption was found in the spectrum. This issue may not fully (or at all) explain the Na scatter, but it is interesting to keep in mind that larger Na abundances could be affected this way. An alternative is significant NLTE effects of the order of 0.4 dex that increase abundances (Baumueller et al. 1998; Takeda et al. 2003; Lind et al. 2011). Line-by-line corrections will be needed to assess whether the overall scatter would decrease; in their absence, at least a global correction should be applied before comparing abundances with model results.

### 4.6. Magnesium

Magnesium is a typical $\alpha$-element. Its abundance is enhanced in halo and dwarf galaxy stars at the [Mg/Fe] $\sim$ 0.4 level. Nevertheless, a number of halo stars have rather strong Mg (and also Si) enhancements. These stars are likely the result of unusual progenitor supernovae as they significantly deviate from the main trend.

It can be expected that a variety of oscillator strengths, log $gf$ values, have been used by the many studies over the last several decades. While the latest measurements by Aldenius et al. (2007) report uncertainties of 9% in $gf$ values, which translates to 0.04 dex in log $gf$, previous studies likely used others, some of which were somewhat uncertain, at least for the Mg $b$ lines. This should be kept in mind because it can lead to systematic differences between studies (depending on which values were used) and hence increased scatter. This is in addition to internal scatter between lines, e.g., between the Mg $b$ lines and the blue Mg triplet lines at 3829–3838 Å, which is often larger than the new log $gf$ uncertainties quoted above.

NLTE effects are similar to those of iron, and yield similar positive corrections for all lines (Mashonkina 2013; Bergemann et al. 2017)

### 4.7. Aluminum and Silicon

Both elements have only two lines available, one of which (in both cases) is significantly blended with CH and the other one is often too weak to be detected. All four lines are in a lower S/N region (3500–4100 Å), which often results in large uncertainties. Three-dimensional and NLTE effects have been studied for Al (Nordlander et al. 2017). They found corrections to be around 0.4 dex. For Si, Mashonkina et al. (2016) and Ezzeddine et al. (2016) investigated NLTE effects. We also caution that for Si abundances, there is also a well-established correlation with effective temperature, e.g., Preston et al. (2006a). Ideal samples for comparison with theoretical models might be stars with similar temperatures.

### 4.8. Potassium

Potassium is not detected in many metal-poor stars down to [Fe/H] $\sim -4.0$. However, often there appear lines at the K line positions which are atmospheric lines that remain in the spectrum if telluric line removal has not been applied (which usually is not necessary when obtaining optical abundances). If these telluric lines were to be mistaken for K lines, then the star becomes potassium enhanced. Original papers should be consulted regarding telluric line removal and other comments. (By the way, potassium-rich stars were once discovered in France after the night assistant at the telescope lit a match in the dome, which resulted in stars displaying "potassium flares" in their spectra. This makes for a good story rather than good model comparison data, although it can be assumed that this issue is not a problem with modern data and unrelated to the telluric lines blending with stellar K lines.)

### 4.9. Calcium

In metal-poor stars, calcium is usually determined from Ca I lines. The strongest one is at 4226 Å, which can still be measured in the most metal-poor stars. However, this line is also blended with iron, which needs to be taken into account. Moreover, it often gives spurious results compared with other Ca I lines in LTE, which is unfortunately made worse when applying NLTE corrections. Other weaker Ca I lines are thus principally preferable.

The Ca II K line is much too strong for abundance measurements except in the few cases of the most iron-poor stars. A few other Ca II lines are available around 3700 Å but are not often used because they are too weak. The Ca II triplet lines are another option but their abundances are known to be strongly affected by NLTE (Mashonkina et al. 2007; Spite et al. 2012). As is the case for basically all strong lines, NLTE corrections are large and highly line dependent. This prevents a simple adjustment to account for NLTE effects. In a heterogeneous sample, it would thus be best to just use weak Ca I abundances.

### 4.10. Scandium

Scandium is detectable in two ionization stages. In metal-poor stars, only Sc II is usually available. Some lines are blended with CH. In the case of carbon-enhanced metal-poor stars, Sc may be unreliable due to severe blending. NLTE corrections for metal-poor stars have not yet been determined for Sc.

### 4.11. Titanium

Titanium is detectable in two ionization stages. In metal-poor stars, mostly Ti II is available. More than a dozen lines are usually available. Regarding NLTE, neutral species are always affected, and ionized species only in a minor way. Hence, Ti I is affected by NLTE (Bergemann 2011; Sitnova et al. 2016) but corrections are similar for all lines and generally well behaved. Ti II is hardly affected and should thus be chosen for abundance comparisons.

### 4.12. Vanadium

Until recently, vanadium was not (yet) an extensively studied element due to missing good oscillator strength (Lawler et al. 2014; Wood et al. 2014). Recent works have yielded some abundances for metal-poor stars with [Fe/H] $< -2.5$ but V lines remain undetectable in the most metal-poor stars. All lines are below 4200 Å, which makes detections more difficult.

### 4.13. Chromium and Manganese

Chromium and manganese are usually detectable in two ionization stages in metal-poor stars. The Cr I abundances typically are about a few tenths of a dex lower than Cr II values. For Mn, Mn I lines with higher excitation potential largely agree with the Mn II lines when the Mn I triplet lines at 4030 Å are excluded. Original papers need to be consulted to learn which lines have been used for a given star.

Both Cr I and Mn I lines are significantly affected by NLTE by several tenths of a dex and thus produce larger abundances (e.g., Bergemann & Gehren 2008; Bergemann & Cescutti 2010) especially at low metallicity. Given that Cr I and Mn I lines are more reliably measured than lines of the ionized species, this is a challenging problem. If possible, abundance from lines of ionized species should be used for comparisons with model results. Otherwise, NLTE-corrected values, when available, based on Cr I and Mn I can be used, or uncorrected abundance with appropriate caution.

### 4.14. Iron

Iron is the element with the most absorption lines in stellar spectra of metal-poor stars. Its abundance is also used as a proxy for the overall metallicity, and thus often regarded to be the most important element to measure and characterize a star. Unfortunately, obtaining accurate and precise Fe abundances is a complex and challenging undertaking.

Iron is detectable in two ionization stages. In metal-poor stars, Fe I is available, but Fe II is often not especially in warmer or more metal-poor stars (but this also depends on the data quality). Statistically speaking, the Fe I abundance can be much more accurately determined than any other abundance given that often more than 150 lines are available, as opposed to $\sim$1–30 lines for the other elements. But Fe I is affected by NLTE (Mashonkina et al. 2011; Bergemann et al. 2012; Sitnova et al. 2015; Ezzeddine et al. 2016; Amarsi et al. 2016b), particularly the most iron-poor stars. Hence, Fe II should principally be chosen for abundance comparisons since it is hardly affected by departures from LTE. However, since the ionization balance between Fe I and Fe II is often used to determine the star's surface gravity (in LTE), the Fe II abundance cannot, in practice, offer an advantage after all. This is also the case if any calibration such as that provided in Frebel et al. (2013) has been applied.

What to do? Future stellar parameter determinations will take NLTE fully into account (e.g., Ezzeddine et al. 2017). This will make stars slightly more metal-rich but would solve the problem. The issue is that these calculations are not yet available for almost all stars. In the meantime, we have to use what is available, keeping in mind the limitations. To minimize systematic uncertainties, Fe II should be used if it is determined independently from the surface gravity (original papers will need to be consulted). The next best choice are NLTE-corrected Fe I abundances. If both of these are not available, LTE Fe I values need to be used. Ezzeddine et al. (2017) have provided a straightforward calibration for adjusting LTE Fe I abundances for NLTE effects. Until NLTE values are available for all stars, this might be an acceptable solution.

### 4.15. Cobalt and Nickel

Cobalt and nickel are often detected in stars with [Fe/H] $< -3.0$. With two exceptions, cobalt lines are located below $\sim$3500 Å, where the S/N is usually low, which increases the abundance uncertainties. Nickel lines are located below $\sim$3600 Å, with two exceptions, with similar uncertainties. Ni I and Ni II lines, when both detected, yield consistent abundances in metal-poor giants and main-sequence TO stars (e.g., Roederer et al. 2016c; Sneden et al. 2016), giving confidence to abundances derived from Ni I. NLTE for Co has been studied by Zhang et al. (2009). However, nothing has been published for Ni yet.

### 4.16. Copper

Cu I has been measured in relatively few metal-poor stars but down to [Fe/H] $\sim -4$. The two main optical lines used are, among others, at 5105.54 and 5782.13 Å. Two resonance lines are present in the near-UV spectral range at 3247 Å and 3273 Å, which actually are strong enough for detection in metal-poor stars. There are also several UV lines (Roederer et al. 2014e). However, Bonifacio et al. (2010) showed that the near-UV lines are affected by 3D corrections under LTE and do not return abundances consistent with those from the optical lines, or with Cu II (Roederer et al. 2014e). NLTE calculations (using a new model atom for Cu) by Andrievsky et al. (2017) show that the abundances determined from the near-UV and UV lines are consistent but agreement with optical lines may only be reached with 3D-NLTE modeling. As such measurements are yet to be computed, original papers need to be consulted to learn which Cu lines were employed and under which assumptions abundance have been determined.

### 4.17. Zinc

Zinc lines can be detected down to [Fe/H] $\sim -4.0$ in red giants (Cayrel et al. 2004; Nissen et al. 2007; Roederer et al. 2014b; and only up to higher metallicities in warmer stars) in the optical wavelength regime. Upper limits in the most metal-poor stars are unfortunately often meaningless because no strong constraints can be derived, especially for the warmer stars. Because of this effect, Zn upper limits are often not reported in papers. This explains the relatively small sample of stars with Zn measurements. A UV Zn line may offer additional Zn measurements in the future for bright stars that can be observed with the *Hubble Space Telescope*. Zinc lines are affected by NLTE (Takeda et al. 2005; R. Ezzeddine et al. 2019, in preparation).

### 4.18. Neutron-capture Element Examples

Neutron-capture elements have the vast majority of lines below 4000 Å where line blending is significant, and data quality is usually low given the reduced stellar flux in combination with the decreased quantum efficiency of the CCD detectors. This means that it is challenging to obtain spectra that are sufficient for detailed studies. Almost all neutron-capture elements present as ionized species, which makes them less sensitive to NLTE effects (Mashonkina et al. 1999; Mashonkina & Gehren 2001). Exceptions are, e.g., Pd, Ag, Cd, Os, Ir, Pt, Au, and Pb, which all present as neutral species.

We now discuss a few representative neutron-capture elements that are most commonly measured. Strontium and barium lines are detected in almost all metal-poor stars and the elements are likely present in all, although possibly in really small amounts (Roederer 2013). In the few exceptions (often dwarf galaxy stars), upper limits are usually still meaningful because of the intrinsic strengths of the Sr 4077 Å and Ba 4554 Å lines. Due to a lack of blue spectra reaching to $\sim$4100 Å, strontium is measured in comparably few dwarf galaxy stars. But there are several red barium lines that are measurable in the red data of dwarf galaxy stars.

Europium is generally only detected in neutron-capture-enriched metal-poor stars, such as *r*-process, *s*-process, or *i*-process stars. The intrinsically weak line at 3819 Å line is the strongest available line but located in the blue part of the spectrum and often difficult to detect. The next strongest line at 4129 Å is thus usually used to identify neutron-capture element-enhanced stars. Overall, this means that upper limits on Eu are often high and thus rather meaningless because no strong constraints can be derived. Because of this, Eu upper limits are usually not reported. This leads to small samples of stars with actual Eu measurements, especially among dwarf galaxies.

### 4.19. Lead

Depending on the type of star, lead can be a straightforward measurement or a huge challenge. In *s*-process metal-poor stars, Pb abundances are high, which makes it possible to clearly detect the only Pb line in the optical at 4057 Å. It is, however, blended with CH, which needs to be taken into account given the fact that *s*-process stars always have large carbon enhancements. In *r*-process stars, the Pb line is hardly detectable and extremely high data quality of S/N $> 300$, preferably in an $R > 40,000$ spectrum, is needed to attempt it. CH blending remains an issue especially when it is unclear whether Pb is actually detected. Pb appears as a neutral species, which means NLTE effects are strong. Mashonkina et al. (2012) calculated corrections of 0.3–0.5 dex depending on the stellar parameters and Pb abundance. Pb in *s*-process stars formed through the operation of the *s*-process at low metallicity. Pb in *r*-process stars can provide confirmation of *r*-process nucleosynthesis calculations because it is the decay product of thorium and uranium.

### 4.20. Thorium and Uranium

Thorium has several heavily blended absorption lines of which the 4019 Å one is the best. It is notably blended with a $^{13}$CH feature, but also with several others. Most reported Th abundances are based on this line. Uranium is only a tiny blend in the wing of a strong iron line and also blended with a CN feature. The detection is very difficult and requires extremely high-quality data ($R > 40,000$, S/N $\sim 300$) to keep observational uncertainties low. NLTE effects are calculated in Mashonkina et al. (2012). Th and U measurements are of great interest for carrying out cosmo-chronometry, given their radioactive nature and long half-lifes of 4.7 and 14 billion years. Cool giants with the largest overabundances in *r*-process elements are the most suitable stars to attempt especially a U measurement for age-dating purposes. Ages very sensitively depend on abundance uncertainties, which makes cosmo-chronometry very challenging.

## 5. Summary

We have described a new web application and database, JINAbase, to query literature chemical abundance results of metal-poor stars. Various selection criteria can be used to select very specific samples tailored to a user's need for comparing data with model predictions or to select suitable comparison samples for ongoing abundance studies. Plotting options and options for downloading the associated data are included. Upon registering with the web app, authors can upload their own results, which will in turn contribute to the body of data staying up to date. We comment on the nucleosynthesis-specific labels (e.g., *r*-process, *s*-process-enhanced) assigned to metal-poor stars and how we utilize them in JINAbase. The frequencies of metal-poor subclasses are then calculated for the available stars in the database. We also presented a brief analysis of the systematic differences between the literature studies to provide general uncertainties that could be used by theoretical models. For astronomers not familiar with the work of spectroscopists and detailed chemical abundance analyses, we provide commentary on the properties of various chemical elements and how their abundances are obtained from absorption lines in the spectra of metal-poor stars to aid in the selection of suitable stellar samples for model comparisons.

## Appendix
## Studies Included in JINAbase

Additional results will be included regularly in the future to keep the JINAbase content up to date. Currently, the studies included are Afşar et al. (2016), Allen et al. (2012), Andrievsky et al. (2009, 2010), Aoki et al. (2001, 2002a, 2002b, 2002c, 2002d, 2005, 2006, 2007a, 2007b, 2007c, 2008, 2009, 2010, 2012, 2013, 2014), Arnone et al. (2005), Barbuy et al. (2005), Barklem et al. (2005), Behara et al. (2010), Bensby et al. (2011), Bergemann et al. (2010), Bergemann & Cescutti (2010), Bonifacio et al. (2009, 2012), Burris et al. (2000), Caffau et al. (2011, 2013), Çalışkan et al. (2014), Carretta et al. (2002), Casey & Schlaufman (2015), Cayrel et al. (2004), Christlieb et al. (2004), Cohen et al. (2003, 2004, 2006, 2007, 2008), Cohen & Huang (2009), Cohen et al. (2013), Collet et al. (2006), Cowan et al. (2002), Cui et al. (2013), Feltzing et al. (2009), François et al. (2016), Frebel et al. (2005, 2006b, 2007a, 2007b, 2008, 2010a, 2010b, 2014, 2015, 2016), Fulbright (2000), Fulbright et al. (2004), Gallagher et al. (2010), García Pérez et al. (2009), Geisler et al. (2005), Gilmore et al. (2013), Gull et al. (2018), Hansen et al. (2011, 2012, 2014, 2015), Hayek et al. (2009), Hill et al. (2002), Hollek et al. (2011, 2015), Honda et al. (2004, 2006, 2007, 2011a, 2011b), Hosford et al. (2009), Howes et al. (2015, 2016), Ishigaki et al. (2010, 2012, 2013, 2014a), Ito et al. (2009, 2013), Ivans et al. (2003, 2005, 2006), Jablonka et al. (2015), Jacobson et al. (2015), Ji et al. (2016a, 2016b), Johnson & Bolte (2002, 2004), Jonsell et al. (2005, 2006), Keller et al. (2014), Kennedy et al. (2014), Kirby et al. (2015), Koch et al. (2008, 2016), Lai et al. (2007, 2008, 2009, 2011), Li et al. (2013, 2015a, 2015b, 2015c), Lucatello et al. (2003), Masseron et al. (2006), Mashonkina et al. (2010), Masseron et al. (2012), Mashonkina et al. (2014), McWilliam et al. (1995), McWilliam (1998), Meléndez et al. (2010, 2016), Norris et al. (1997a, 1997b, 1997c, 2000, 2001, 2002, 2007, 2010, 2012), Placco et al. (2013, 2014a, 2014b, 2015a, 2015b), Preston & Sneden (2000, 2001), Preston et al. (2006b), Ren et al. (2012), Rich & Boesgaard (2009), Roederer et al. (2008, 2009, 2010, 2012a, 2012b, 2014a, 2014b, 2014c, 2014d, 2014e, 2016b, 2016c), Ruchti et al. (2011), Ryan et al. (1991, 1996), Saito et al. (2009), Schuler et al. (2007), Shetrone et al. (2001, 2003, 2013), Simon et al. (2010, 2015), Siqueira Mello et al. (2012, 2014), Sivarani et al. (2004, 2006), Starkenburg et al. (2013), Skúladóttir et al. (2015), Smiljanic et al. (2009), Sneden et al. (2003, 2016), Spite et al. (2000, 2011, 2012, 2013, 2014), Susmitha Rani et al. (2016), Tafelmeyer et al. (2010), Takeda & Takada-Hidai (2011), Tan et al. (2009), Venn et al. (2012), Westin et al. (2000), Yong et al. (2013), Zacs et al. (1998), and Zhang et al. (2009).

## ORCID iDs

Anna Frebel ⓞ https://orcid.org/0000-0002-2139-7145

## References

Afşar, M., Sneden, C., Frebel, A., et al. 2016, ApJ, 819, 103
Aldenius, M., Tanner, J. D., Johansson, S., Lundberg, H., & Ryan, S. G. 2007, A&A, 461, 767
Allen, D. M., Ryan, S. G., Rossi, S., Beers, T. C., & Tsangarides, S. A. 2012, A&A, 548, A34
Amarsi, A. M., Asplund, M., Collet, R., & Leenaarts, J. 2016a, MNRAS, 455, 3735
Amarsi, A. M., Lind, K., Asplund, M., Barklem, P. S., & Collet, R. 2016b, MNRAS, 463, 1518
Andrievsky, S., Bonifacio, P., Caffau, E., et al. 2017, arXiv:1709.08619
Andrievsky, S. M., Spite, M., Korotin, S. A., et al. 2009, A&A, 494, 1083
Andrievsky, S. M., Spite, M., Korotin, S. A., et al. 2010, A&A, 509, A88
Aoki, W., Ando, H., Honda, S., et al. 2002a, PASJ, 54, 427
Aoki, W., Arimoto, N., Sadakane, K., et al. 2009, A&A, 502, 569
Aoki, W., Beers, T. C., Christlieb, N., et al. 2007a, ApJ, 655, 492
Aoki, W., Beers, T. C., Honda, S., & Carollo, D. 2010, ApJL, 723, L201
Aoki, W., Beers, T. C., Lee, Y. S., et al. 2013, AJ, 145, 13
Aoki, W., Beers, T. C., Sivarani, T., et al. 2008, ApJ, 678, 1351
Aoki, W., Frebel, A., Christlieb, N., et al. 2006, ApJ, 639, 897
Aoki, W., Honda, S., Beers, T. C., et al. 2005, ApJ, 632, 611
Aoki, W., Honda, S., Beers, T. C., et al. 2007b, ApJ, 660, 747
Aoki, W., Honda, S., Sadakane, K., & Arimoto, N. 2007c, PASJ, 59, L15
Aoki, W., Ito, H., & Tajitsu, A. 2012, ApJL, 751, L6
Aoki, W., Norris, J. E., Ryan, S. G., Beers, T. C., & Ando, H. 2002b, ApJ, 567, 1166
Aoki, W., Norris, J. E., Ryan, S. G., Beers, T. C., & Ando, H. 2002c, ApJL, 576, L141
Aoki, W., Norris, J. E., Ryan, S. G., Beers, T. C., & Ando, H. 2002d, PASJ, 54, 933
Aoki, W., Ryan, S. G., Norris, J. E., et al. 2001, ApJ, 561, 346
Aoki, W., Tominaga, N., Beers, T. C., Honda, S., & Lee, Y. S. 2014, Sci, 345, 912

Arnone, E., Ryan, S. G., Argast, D., Norris, J. E., & Beers, T. C. 2005, A&A, 430, 507
Barbuy, B., Spite, M., Spite, F., et al. 2005, A&A, 429, 1031
Barklem, P. S., Christlieb, N., Beers, T. C., et al. 2005, A&A, 439, 129
Baumueller, D., Butler, K., & Gehren, T. 1998, A&A, 338, 637
Beers, T. C., Chiba, M., Yoshii, Y., et al. 2000, AJ, 119, 2866
Beers, T. C., & Christlieb, N. 2005, ARA&A, 43, 531
Behara, N. T., Bonifacio, P., Ludwig, H.-G., et al. 2010, A&A, 513, A72
Bensby, T., Adén, D., Meléndez, J., et al. 2011, A&A, 533, A134
Bergemann, M. 2011, MNRAS, 413, 2184
Bergemann, M., & Cescutti, G. 2010, A&A, 522, A9
Bergemann, M., Collet, R., Amarsi, A. M., et al. 2017, ApJ, 847, 15
Bergemann, M., & Gehren, T. 2008, A&A, 492, 823
Bergemann, M., Lind, K., Collet, R., Magic, Z., & Asplund, M. 2012, MNRAS, 427, 27
Bergemann, M., Pickering, J. C., & Gehren, T. 2010, MNRAS, 401, 1334
Bisterzo, S., Gallino, R., Straniero, O., Cristallo, S., & Käppeler, F. 2012, MNRAS, 422, 849
Bonifacio, P., Caffau, E., & Ludwig, H.-G. 2010, A&A, 524, A96
Bonifacio, P., Sbordone, L., Caffau, E., et al. 2012, A&A, 542, A87
Bonifacio, P., Spite, M., Cayrel, R., et al. 2009, A&A, 501, 519
Bromm, V., & Larson, R. B. 2004, ARA&A, 42, 79
Burris, D. L., Pilachowski, C. A., Armandroff, T. E., et al. 2000, ApJ, 544, 302
Caffau, E., Bonifacio, P., François, P., et al. 2011, Msngr, 146, 28
Caffau, E., Bonifacio, P., François, P., et al. 2013, A&A, 560, A15
Çalışkan, Ş., Caffau, E., Bonifacio, P., et al. 2014, A&A, 571, A62
Carollo, D., Beers, T. C., Lee, Y. S., et al. 2007, Natur, 450, 1020
Carretta, E., Gratton, R., Cohen, J. G., Beers, T. C., & Christlieb, N. 2002, AJ, 124, 481
Casey, A. R., & Schlaufman, K. C. 2015, ApJ, 809, 110
Cayrel, R., Depagne, E., Spite, M., et al. 2004, A&A, 416, 1117
Christlieb, N., Gustafsson, B., Korn, A. J., et al. 2004, ApJ, 603, 708
Cohen, J. G., Christlieb, N., McWilliam, A., et al. 2004, ApJ, 612, 1107
Cohen, J. G., Christlieb, N., McWilliam, A., et al. 2008, ApJ, 672, 320
Cohen, J. G., Christlieb, N., Qian, Y.-Z., & Wasserburg, G. J. 2003, ApJ, 588, 1082
Cohen, J. G., Christlieb, N., Thompson, I., et al. 2013, ApJ, 778, 56
Cohen, J. G., & Huang, W. 2009, ApJ, 701, 1053
Cohen, J. G., McWilliam, A., Christlieb, N., et al. 2007, ApJL, 659, L161
Cohen, J. G., McWilliam, A., Shectman, S., et al. 2006, AJ, 132, 137
Collet, R., Asplund, M., & Trampedach, R. 2006, ApJL, 644, L121
Copeland, R. 2008, Essential Sqlalchemy (1st ed.; Sebastopol, CA: O'Reilly Media)
Côté, B., Belczynski, K., Fryer, C. L., et al. 2017, ApJ, 836, 230
Cowan, J. J., Sneden, C., Burles, S., et al. 2002, ApJ, 572, 861
Crosby, B. D., O'Shea, B. W., Smith, B. D., Turk, M. J., & Hahn, O. 2013, ApJ, 773, 108
Cui, W. Y., Sivarani, T., & Christlieb, N. 2013, A&A, 558, A36
Denissenkov, P. A., Herwig, F., Battino, U., et al. 2017, ApJL, 834, L10
Ezzeddine, R., Frebel, A., & Plez, B. 2017, ApJ, 847, 142
Ezzeddine, R., Plez, B., Merle, T., Gebran, M., & Thévenin, F. 2016, arXiv:1612.09302
Feltzing, S., Eriksson, K., Kleyna, J., & Wilkinson, M. I. 2009, A&A, 508, L1
François, P., Monaco, L., Bonifacio, P., et al. 2016, A&A, 588, A7
Frebel, A. 2010, AN, 331, 474
Frebel, A. 2018, arXiv:1806.08955
Frebel, A., Aoki, W., Christlieb, N., et al. 2005, Natur, 434, 871
Frebel, A., Casey, A. R., Jacobson, H. R., & Yu, Q. 2013, ApJ, 769, 57
Frebel, A., Chiti, A., Ji, A. P., Jacobson, H. R., & Placco, V. M. 2015, ApJL, 810, L27
Frebel, A., Christlieb, N., Norris, J. E., et al. 2006a, ApJ, 652, 1585
Frebel, A., Christlieb, N., Norris, J. E., et al. 2007a, ApJL, 660, L117
Frebel, A., Christlieb, N., Norris, J. E., Aoki, W., & Asplund, M. 2006b, ApJL, 638, L17
Frebel, A., Collet, R., Eriksson, K., Christlieb, N., & Aoki, W. 2008, ApJ, 684, 588
Frebel, A., Kirby, E. N., & Simon, J. D. 2010a, Natur, 464, 72
Frebel, A., Norris, J. E., Aoki, W., et al. 2007b, ApJ, 658, 534
Frebel, A., Norris, J. E., Gilmore, G., & Wyse, R. F. G. 2016, ApJ, 826, 110
Frebel, A., Simon, J. D., Geha, M., & Willman, B. 2010b, ApJ, 708, 560
Frebel, A., Simon, J. D., & Kirby, E. N. 2014, ApJ, 786, 74
Fulbright, J. P. 2000, AJ, 120, 1841
Fulbright, J. P., Rich, R. M., & Castro, S. 2004, ApJ, 612, 447
Gallagher, A. J., Caffau, E., Bonifacio, P., et al. 2016, A&A, 593, A48
Gallagher, A. J., Caffau, E., Bonifacio, P., et al. 2017, A&A, 598, L10

Gallagher, A. J., Ryan, S. G., García Pérez, A. E., & Aoki, W. 2010, A&A, 523, A24
García Pérez, A. E., Allende Prieto, C., Holtzman, J. A., et al. 2016, AJ, 151, 144
García Pérez, A. E., Aoki, W., Inoue, S., et al. 2009, A&A, 504, 213
Geisler, D., Smith, V. V., Wallerstein, G., Gonzalez, G., & Charbonnel, C. 2005, AJ, 129, 1428
Gilmore, G., Norris, J. E., Monaco, L., et al. 2013, ApJ, 763, 61
Greif, T. H., Glover, S. C. O., Bromm, V., & Klessen, R. S. 2010, ApJ, 716, 510
Grinberg, M. 2014, Flask Web Development: Developing Web Applications with Python (1st ed.; Sebastopolo, CA: O'Reilly Media, Inc.)
Gull, M., Frebel, A., Cain, M. G., et al. 2018, arXiv:1806.00645
Hampel, M., Stancliffe, R. J., Lugaro, M., & Meyer, B. S. 2016, ApJ, 831, 171
Hansen, C. J., Nordström, B., Bonifacio, P., et al. 2011, A&A, 527, A65
Hansen, C. J., Primas, F., Hartman, H., et al. 2012, A&A, 545, A31
Hansen, T., Hansen, C. J., Christlieb, N., et al. 2014, ApJ, 787, 162
Hansen, T., Hansen, C. J., Christlieb, N., et al. 2015, ApJ, 807, 173
Hansen, T. T., Holmbeck, E. M., Beers, T. C., et al. 2018, ApJ, 858, 92
Hayek, W., Wiesendahl, U., Christlieb, N., et al. 2009, A&A, 504, 511
Heger, A., & Woosley, S. E. 2010, ApJ, 724, 341
Heiter, U., Jofré, P., Gustafsson, B., et al. 2015, A&A, 582, A49
Hill, V., Plez, B., Cayrel, R., et al. 2002, A&A, 387, 560
Hollek, J. K., Frebel, A., Placco, V. M., et al. 2015, ApJ, 814, 121
Hollek, J. K., Frebel, A., Roederer, I. U., et al. 2011, ApJ, 742, 54
Honda, S., Aoki, W., Arimoto, N., & Sadakane, K. 2011a, PASJ, 63, 523
Honda, S., Aoki, W., Beers, T. C., & Takada-Hidai, M. 2011b, ApJ, 730, 77
Honda, S., Aoki, W., Ishimaru, Y., & Wanajo, S. 2007, ApJ, 666, 1189
Honda, S., Aoki, W., Ishimaru, Y., Wanajo, S., & Ryan, S. G. 2006, ApJ, 643, 1180
Honda, S., Aoki, W., Kajino, T., et al. 2004, ApJ, 607, 474
Hosford, A., Ryan, S. G., García Pérez, A. E., Norris, J. E., & Olive, K. A. 2009, A&A, 493, 601
Howes, L. M., Asplund, M., Keller, S. C., et al. 2016, MNRAS, 460, 884
Howes, L. M., Casey, A. R., Asplund, M., et al. 2015, Natur, 527, 484
Ishigaki, M., Chiba, M., & Aoki, W. 2010, PASJ, 62, 143
Ishigaki, M. N., Aoki, W., Arimoto, N., & Okamoto, S. 2014a, A&A, 562, A146
Ishigaki, M. N., Aoki, W., & Chiba, M. 2013, ApJ, 771, 67
Ishigaki, M. N., Chiba, M., & Aoki, W. 2012, ApJ, 753, 64
Ishigaki, M. N., Tominaga, N., Kobayashi, C., & Nomoto, K. 2014b, ApJL, 792, L32
Ito, H., Aoki, W., Beers, T. C., et al. 2013, ApJ, 773, 33
Ito, H., Aoki, W., Honda, S., & Beers, T. C. 2009, ApJL, 698, L37
Ivans, I. I., Simmerer, J., Sneden, C., et al. 2006, ApJ, 645, 613
Ivans, I. I., Sneden, C., Gallino, R., Cowan, J. J., & Preston, G. W. 2005, ApJL, 627, L145
Ivans, I. I., Sneden, C., James, C. R., et al. 2003, ApJ, 592, 906
Jablonka, P., North, P., Mashonkina, L., et al. 2015, A&A, 583, A67
Jacobson, H. R., Keller, S., Frebel, A., et al. 2015, ApJ, 807, 171
Ji, A. P., Frebel, A., Chiti, A., & Simon, J. D. 2016a, Natur, 531, 610
Ji, A. P., Frebel, A., Simon, J. D., & Geha, M. 2016b, ApJ, 817, 41
Jofré, P., Heiter, U., Soubiran, C., et al. 2014, A&A, 564, A133
Johnson, J. A. 2002, ApJS, 139, 219
Johnson, J. A., & Bolte, M. 2002, ApJL, 579, L87
Johnson, J. A., & Bolte, M. 2004, ApJ, 605, 462
Jonsell, K., Barklem, P. S., Gustafsson, B., et al. 2006, A&A, 451, 651
Jonsell, K., Edvardsson, B., Gustafsson, B., et al. 2005, A&A, 440, 321
Karakas, A. I. 2010, MNRAS, 403, 1413
Keller, S. C., Bessell, M. S., Frebel, A., et al. 2014, Natur, 506, 463
Kennedy, C. R., Stancliffe, R. J., Kuehn, C., et al. 2014, ApJ, 787, 6
Kim, Y.-C., Demarque, P., Yi, S. K., & Alexander, D. R. 2002, ApJS, 143, 499
Kirby, E. N., Guo, M., Zhang, A. J., et al. 2015, ApJ, 801, 125
Koch, A., McWilliam, A., Grebel, E. K., Zucker, D. B., & Belokurov, V. 2008, ApJL, 688, L13
Koch, A., McWilliam, A., Preston, G. W., & Thompson, I. B. 2016, A&A, 587, 124
Korn, A. J., Grundahl, F., Richard, O., et al. 2006, Natur, 442, 657
Lai, D. K., Bolte, M., Johnson, J. A., et al. 2008, ApJ, 681, 1524
Lai, D. K., Johnson, J. A., Bolte, M., & Lucatello, S. 2007, ApJ, 667, 1185
Lai, D. K., Lee, Y. S., Bolte, M., et al. 2011, ApJ, 738, 51
Lai, D. K., Rockosi, C. M., Bolte, M., et al. 2009, ApJL, 697, L63
Lawler, J. E., Wood, M. P., Den Hartog, E. A., et al. 2014, ApJS, 215, 20
Li, H., Aoki, W., Zhao, G., et al. 2015a, PASJ, 67, 84
Li, H.-N., Aoki, W., Honda, S., et al. 2015b, RAA, 15, 1264

Li, H. N., Ludwig, H.-G., Caffau, E., Christlieb, N., & Zhao, G. 2013, ApJ, 765, 51

Li, H.-N., Zhao, G., Christlieb, N., et al. 2015c, ApJ, 798, 110

Lind, K., Asplund, M., Barklem, P. S., & Belyaev, A. K. 2011, A&A, 528, A103

Lind, K., Melendez, J., Asplund, M., Collet, R., & Magic, Z. 2013, A&A, 554, A96

Lucatello, S., Beers, T. C., Christlieb, N., et al. 2006, ApJL, 652, L37

Lucatello, S., Gratton, R., Cohen, J. G., et al. 2003, AJ, 125, 875

Lugaro, M., de Mink, S. E., Izzard, R. G., et al. 2008, A&A, 484, L27

Mashonkina, L. 2013, A&A, 550, A28

Mashonkina, L., Christlieb, N., Barklem, P. S., et al. 2010, A&A, 516, A46

Mashonkina, L., Christlieb, N., & Eriksson, K. 2014, A&A, 569, A43

Mashonkina, L., & Gehren, T. 2001, A&A, 376, 232

Mashonkina, L., Gehren, T., & Bikmaev, I. 1999, A&A, 343, 519

Mashonkina, L., Gehren, T., Shi, J.-R., Korn, A. J., & Grupp, F. 2011, A&A, 528, A87

Mashonkina, L., Korn, A. J., & Przybilla, N. 2007, A&A, 461, 261

Mashonkina, L., Ryabtsev, A., & Frebel, A. 2012, A&A, 540, A98

Mashonkina, L. I., Belyaev, A. K., & Shi, J.-R. 2016, AstL, 42, 366

Masseron, T., Johnson, J. A., Lucatello, S., et al. 2012, ApJ, 751, 14

Masseron, T., van Eck, S., Famaey, B., et al. 2006, A&A, 455, 1059

Matteucci, F. 2012, Chemical Evolution of Galaxies (Berlin: Springer)

McKinney, W. 2010, in Proc. 9th Python in Science Conf., ed. S. van der Walt & J. Millman, 51, http://conference.scipy.org/proceedings/scipy2010/mckinney.html

McWilliam, A. 1998, AJ, 115, 1640

McWilliam, A., Preston, G. W., Sneden, C., & Searle, L. 1995, AJ, 109, 2757

Meléndez, J., Casagrande, L., Ramírez, I., Asplund, M., & Schuster, W. J. 2010, A&A, 515, L3

Meléndez, J., Placco, V. M., Tucci-Maia, M., et al. 2016, A&A, 585, L5

Minchev, I., Chiappini, C., & Martig, M. 2014, A&A, 572, A92

Nissen, P. E., Akerman, C., Asplund, M., et al. 2007, A&A, 469, 319

Nomoto, K., Kobayashi, C., & Tominaga, N. 2013, ARA&A, 51, 457

Nordlander, T., Amarsi, A. M., Lind, K., et al. 2017, A&A, 597, A6

Norris, J. E., Beers, T. C., & Ryan, S. G. 2000, ApJ, 540, 456

Norris, J. E., Christlieb, N., Bessell, M. S., et al. 2012, ApJ, 753, 150

Norris, J. E., Christlieb, N., Korn, A. J., et al. 2007, ApJ, 670, 774

Norris, J. E., Ryan, S. G., & Beers, T. C. 1997a, ApJ, 488, 350

Norris, J. E., Ryan, S. G., & Beers, T. C. 1997b, ApJL, 489, L169

Norris, J. E., Ryan, S. G., & Beers, T. C. 2001, ApJ, 561, 1034

Norris, J. E., Ryan, S. G., Beers, T. C., Aoki, W., & Ando, H. 2002, ApJL, 569, L107

Norris, J. E., Ryan, S. G., Beers, T. C., & Deliyannis, C. P. 1997c, ApJ, 485, 370

Norris, J. E., Yong, D., Gilmore, G., & Wyse, R. F. G. 2010, ApJ, 711, 350

O'Shea, B. W., & Norman, M. L. 2007, ApJ, 654, 66

Placco, V. M., Beers, T. C., Ivans, I. I., et al. 2015a, ApJ, 812, 109

Placco, V. M., Beers, T. C., Roederer, I. U., et al. 2014a, ApJ, 790, 34

Placco, V. M., Frebel, A., Beers, T. C., et al. 2013, ApJ, 770, 104

Placco, V. M., Frebel, A., Beers, T. C., et al. 2014b, ApJ, 781, 40

Placco, V. M., Frebel, A., Beers, T. C., & Stancliffe, R. J. 2014c, ApJ, 797, 21

Placco, V. M., Frebel, A., Lee, Y. S., et al. 2015b, ApJ, 809, 136

Preston, G. W., & Sneden, C. 2000, AJ, 120, 1014

Preston, G. W., & Sneden, C. 2001, AJ, 122, 1545

Preston, G. W., Sneden, C., Thompson, I. B., Shectman, S. A., & Burley, G. S. 2006a, AJ, 132, 85

Preston, G. W., Thompson, I. B., Sneden, C., Stachowski, G., & Shectman, S. A. 2006b, AJ, 132, 1714

Ren, J., Christlieb, N., & Zhao, G. 2012, A&A, 537, A118

Rich, J. A., & Boesgaard, A. M. 2009, ApJ, 701, 1519

Roederer, I. U. 2013, A.J., 145, 26

Roederer, I. U., Cowan, J. J., Preston, G. W., et al. 2014a, MNRAS, 445, 2970

Roederer, I. U., Frebel, A., Shetrone, M. D., et al. 2008, ApJ, 679, 1549

Roederer, I. U., Jacobson, H. R., Thanathibodee, T., Frebel, A., & Toller, E. 2014b, ApJ, 797, 69

Roederer, I. U., Karakas, A. I., Pignatari, M., & Herwig, F. 2016a, ApJ, 821, 37

Roederer, I. U., Kratz, K.-L., Frebel, A., et al. 2009, ApJ, 698, 1963

Roederer, I. U., Lawler, J. E., Cowan, J. J., et al. 2012a, ApJL, 747, L8

Roederer, I. U., Lawler, J. E., Sobeck, J. S., et al. 2012b, ApJS, 203, 27

Roederer, I. U., Mateo, M., Bailey, J. I., III, et al. 2016b, AJ, 151, 82

Roederer, I. U., Placco, V. M., & Beers, T. C. 2016c, ApJL, 824, L19

Roederer, I. U., Preston, G. W., Thompson, I. B., et al. 2014c, AJ, 147, 136

Roederer, I. U., Preston, G. W., Thompson, I. B., Shectman, S. A., & Sneden, C. 2014d, ApJ, 784, 158

Roederer, I. U., Schatz, H., Lawler, J. E., et al. 2014e, ApJ, 791, 32

Roederer, I. U., Sneden, C., Thompson, I. B., Preston, G. W., & Shectman, S. A. 2010, ApJ, 711, 573

Rossi, S., Beers, T. C., & Sneden, C. 1999, in ASP Conf. Ser. 165: The Third Stromlo Symposium: The Galactic Halo, ed. B. K. Gibson, R. S. Axelrod, & M. E. Putman (San Francisco, CA: ASP), 264

Rossum, G. 1995, Python Reference Manual, Tech. Rep. CS-R9525

Ruchti, G. R., Fulbright, J. P., Wyse, R. F. G., et al. 2011, ApJ, 743, 107

Ryan, S. G., Norris, J. E., & Beers, T. C. 1996, ApJ, 471, 254

Ryan, S. G., Norris, J. E., & Bessell, M. S. 1991, AJ, 102, 303

Saito, Y.-J., Takada-Hidai, M., Honda, S., & Takeda, Y. 2009, PASJ, 61, 549

Schuler, S. C., Cunha, K., Smith, V. V., et al. 2007, ApJL, 667, L81

Shetrone, M., Venn, K. A., Tolstoy, E., et al. 2003, AJ, 125, 684

Shetrone, M. D., Côté, P., & Sargent, W. L. W. 2001, ApJ, 548, 592

Shetrone, M. D., Smith, G. H., Stanford, L. M., Siegel, M. H., & Bond, H. E. 2013, AJ, 145, 123

Simmerer, J., Sneden, C., Cowan, J. J., et al. 2004, ApJ, 617, 1091

Simon, J. D., Frebel, A., McWilliam, A., Kirby, E. N., & Thompson, I. B. 2010, ApJ, 716, 446

Simon, J. D., Jacobson, H. R., Frebel, A., et al. 2015, ApJ, 802, 93

Siqueira Mello, C., Barbuy, B., Spite, M., & Spite, F. 2012, A&A, 548, A42

Siqueira Mello, C., Hill, V., Barbuy, B., et al. 2014, A&A, 565, A93

Sitnova, T., Zhao, G., Mashonkina, L., et al. 2015, ApJ, 808, 148

Sitnova, T. M., Mashonkina, L. I., & Ryabchikova, T. A. 2016, MNRAS, 461, 1000

Sivarani, T., Beers, T. C., Bonifacio, P., et al. 2006, A&A, 459, 125

Sivarani, T., Bonifacio, P., Molaro, P., et al. 2004, A&A, 413, 1073

Skúladóttir, Á, Tolstoy, E., Salvadori, S., et al. 2015, A&A, 574, A129

Smiljanic, R., Korn, A. J., Bergemann, M., et al. 2014, A&A, 570, A122

Smiljanic, R., Pasquini, L., Bonifacio, P., et al. 2009, A&A, 499, 103

Sneden, C., Cowan, J. J., Kobayashi, C., et al. 2016, ApJ, 817, 53

Sneden, C., Cowan, J. J., Lawler, J. E., et al. 2003, ApJ, 591, 936

Spite, M., Andrievsky, S. M., Spite, F., et al. 2012, A&A, 541, A143

Spite, M., Caffau, E., Andrievsky, S. M., et al. 2011, A&A, 528, A9

Spite, M., Caffau, E., Bonifacio, P., et al. 2013, A&A, 552, A107

Spite, M., Depagne, E., Nordström, B., et al. 2000, A&A, 360, 1077

Spite, M., Spite, F., Bonifacio, P., et al. 2014, A&A, 571, A40

Starkenburg, E., Hill, V., Tolstoy, E., et al. 2013, A&A, 549, A88

Suda, T., Katsuta, Y., Yamada, S., et al. 2008, PASJ, 60, 1159

Susmitha Rani, A., Sivarani, T., Beers, T. C., et al. 2016, MNRAS, 458, 2648

Tafelmeyer, M., Jablonka, P., Hill, V., et al. 2010, A&A, 524, A58

Takeda, Y., Hashimoto, O., Taguchi, H., et al. 2005, PASJ, 57, 751

Takeda, Y., & Takada-Hidai, M. 2011, PASJ, 63, 537

Takeda, Y., Zhao, G., Takada-Hidai, M., et al. 2003, ChJAA, 3, 316

Tan, K. F., Shi, J. R., & Zhao, G. 2009, MNRAS, 392, 205

Team, B. D. 2014, Bokeh: Python Library for Interactive Visualization

van der Walt, S., Colbert, S. C., & Varoquaux, G. 2011, arXiv:1102.1523

Venn, K. A., Shetrone, M. D., Irwin, M. J., et al. 2012, ApJ, 751, 102

Vlasov, A. D., Metzger, B. D., Lippuner, J., Roberts, L. F., & Thompson, T. A. 2017, MNRAS, 468, 1522

Wanajo, S. 2013, ApJL, 770, L22

Westin, J., Sneden, C., Gustafsson, B., & Cowan, J. J. 2000, ApJ, 530, 783

Winteler, C., Käppeli, R., Perego, A., et al. 2012, ApJL, 750, L22

Wise, J. H., Turk, M. J., Norman, M. L., & Abel, T. 2012, ApJ, 745, 50

Wood, M. P., Lawler, J. E., Den Hartog, E. A., Sneden, C., & Cowan, J. J. 2014, ApJS, 215, 20

Yong, D., Norris, J. E., Bessell, M. S., et al. 2013, ApJ, 762, 26

Zacs, L., Nissen, P. E., & Schuster, W. J. 1998, A&A, 337, 216

Zhang, L., Ishigaki, M., Aoki, W., Zhao, G., & Chiba, M. 2009, ApJ, 706, 1095